Inorganic Chemistry

pubs.acs.org/IC Forum Article

Effects of Ligand Substitution on the Optical and Electrochemical Properties of (Pyridinedipyrrolide)zirconium Photosensitizers

Yu Zhang, Dylan C. Leary, Anne M. Belldina, Jeffrey L. Petersen, and Carsten Milsmann*



Cite This: Inorg. Chem. 2020, 59, 14716–14730



ACCESS

Metrics & More

Article Recommendations

Supporting Information

ABSTRACT: A series of seven bis(pyridinedipyrrolide)zirconium complexes, $Zr(^{R_1}PDP^{R_2})_2$, where $[^{R_1}PDP^{R_2}]^{2-}$ is the doubly deprotonated form of [2,6-bis(5- R_1 -3- R_2 -1H-pyrrol-2-yl)pyridine], were prepared and characterized in solution by NMR, UV/vis absorption, and emission spectroscopy and cyclic voltammetry. The molecular structures were determined by single-crystal X-ray crystallography. All complexes exhibit remarkably long emission lifetimes ($\tau = 190-576~\mu s$) with high quantum efficiencies ($\Phi_{PL} = 100-100$

Reduction Potential:
-1.85 to -2.42 V vs Fc^{+/0}

Color:
abs. 483 to 547 nm
em. 568 to 629 nm
QY 0.10 to 0.38

Long-lived Excited State:
190 to 576 µs

0.10-0.38) upon excitation with visible light in a benzene solution. The substituents on the pyrrolide rings were shown to have significant effects on the photoluminescence and electrochemical properties of these compounds. The R_2 substituents ($R_2 = H$, Me, Ph, or C_6F_5) show only limited effects on the absorption and emission profiles of the complexes but allow systematic tuning of the ground- and excited-state redox potentials over a range of almost 600 mV. The R_1 substituents ($R_1 = H$, Me, Ph, or 2,4,6-Me₃Ph) influence both the optical and electrochemical properties through electronic effects. Additionally, the R_1 substituents have profound consequences for the structural flexibility and overall stability of the compounds. Distortions of the $Zr(PDP)_2$ core from idealized D_{2d} symmetry in the solid state can be traced to the steric profiles of the R^1 substituents and correlate with the observed Stokes shifts for each compound. The complex with the smallest ligand system, $Zr(^HPDP^H)_2$, coordinates two additional solvent molecules in a tetrahydrofuran (THF) solution, which allowed the isolation of photoluminescent, eight-coordinate $Zr(^HPDP^H)_2(THF)_2$. The photoredox catalytic dehalogenation of aryl iodides and aryl chlorides using the most reducing derivative, $Zr(^{Me}PDP^{Me})_2$, highlights the potential of $Zr(PDP)_2$ photosensitizers to promote challenging reductive transformations under mild conditions upon excitation with green light.

■ INTRODUCTION

Transition-metal photosensitizers play an important role in a wide range of chemical applications. Dye-sensitized solar cells^{1–4} and organic light-emitting diodes^{5,6} often rely on the ability of molecular inorganic chromophores to convert light into electrical energy (and vice versa) and are critical components of a sustainable and efficient energy economy. At the same time, light-to-chemical energy conversion using transition-metal complexes is central to the rapidly expanding fields of photoredox catalysis^{7–15} and solar fuel generation, ^{16,17} which have the potential to revolutionize the production of fine and commodity chemicals. Finally, the ability of photosensitizers to generate highly reactive species under otherwise mild conditions through irradiation with visible light at high temporal and spatial resolution is exploited in photodynamic therapy.¹⁸

Because each application within this wide range of technologies has its distinct set of performance critical parameters—e.g., specific absorption or emission profiles, range of redox potentials, or lifetime and quantum yield demands—careful control over the properties of photosensitizers is crucial. In this aspect, molecular transitionmetal photosensitizers offer a distinct advantage over semiconductor or other solid-state materials because their proper-

ties can be more readily tuned through systematic ligand modifications using the versatile toolboxes of synthetic organic and coordination chemistry.

One generally accepted design principle for transition-metal photosensitizers is rigidification of the ligand framework. The reduction of nonradiative decay pathways resulting from vibrational modes can result in significant improvements of the luminescence quantum yields and excited-state lifetimes. ¹⁹ While this approach has been studied for a variety of transition-metal chromophores, it is most dramatically reflected in the optical properties of copper(I) bisphenanthroline complexes, in which long-lived luminescence is enabled through the introduction of sterically demanding substituents that prevent excited-state Jahn—Teller flattening from tetrahedral to square-planar geometry. ^{20–23} A second concept, most relevant to first-row transition-metal photosensitizers, is the

Special Issue: Light-Controlled Reactivity of Metal Complexes

Received: August 6, 2020 Published: September 25, 2020





Scheme 1. Synthetic Routes to New H₂^{R₁}PDP^{R₂} Derivatives

suppression of detrimental metal-centered (MC) excited states, which similarly improves the luminescence quantum yields and results in longer lifetimes. This approach has been shown for chromium(0) isocyanide complexes featuring metal-to-ligand charge-transfer (MLCT) excited states, ^{24,25} chromium(III) complexes operating via d—d excitation, ^{26–28} and iron(II) and iron(III) complexes exhibiting MLCT and ligand-to-metal charge-transfer (LMCT) states, respectively. ^{29–32}

Aside from structural modifications, the introduction of electron-donating or -withdrawing substituents into the ligand scaffold can have a direct influence on the electronic structure of the photosensitizer, which ideally allows systematic control over the absorption and emission profiles and electron-transfer properties in the ground and excited states.^{33–35} The influence of the substituents on the frontier molecular orbitals can be either indirect through ligand-field effects on the metal d orbitals (for MLCT, LMCT, or MC states) or direct if one or both of the molecular orbital(s) involved in the corresponding transition exhibit significant ligand character. The latter is the case for complexes with MLCT, LMCT, or ligand-to-ligand charge-transfer excited states.

Recent work in our group has focused on the development of photoluminescent zirconium complexes with pyridinedipyrrolide (PDP) ligands.^{36–38} The bis-ligand complexes Zr-(PDP)₂ exhibit remarkably long excited-state lifetimes that allow facile photoinduced single-electron transfer under photoredox catalytic conditions. These compounds expand the limited pool of photosensitizers utilizing excited states with high LMCT character^{39–49} and demonstrate the utility of more Earth-abundant early transition metals in photochemical applications, which are otherwise dominated by precious metal chromophores. 15,50,51 Initial investigations of the ligand substituent effects resulted in the discovery of Zr(MesPDPPh)2 based on the sterically demanding ligand precursor 2,6-bis [5-(2,4,6-trimethylphenyl)-3-phenyl-1*H*-pyrrol-2-yl]pyridine (H₂MesPDP^{Ph}).³⁸ This complex showed a substantially improved photoluminescence quantum yield and markedly higher stability under ambient conditions compared to the initially reported analogue Zr(MePDPPh)2, in which the 2,4,6trimethylphenyl substituents on the pyrroles are replaced by much smaller methyl substituents. The increased stability of $Zr(^{Mes}PDP^{Ph})_2$ allowed detailed photophysical studies that revealed that the long emission lifetime of $Zr(PDP)_2$ complexes can be attributed to thermally activated delayed fluorescence (TADF).

In this work, we describe the influence of pyrrole substitution at the 3 and 5 positions of these N-heterocycles on the optical and electrochemical properties of $Zr(PDP)_2$ complexes. Solid-state molecular structures obtained by single-crystal X-ray diffraction show a major influence of the substituents at the 5 position of the pyrroles on the overall geometry of the complexes, which results in considerable changes to the optical properties. In contrast, substitution at the 3 position produces only minor alterations in the absorption and emission profiles but allows systematic tuning of the redox properties of $Zr(PDP)_2$ complexes over a range of more than 0.5 V.

■ RESULTS AND DISCUSSION

Ligand Synthesis. For unambiguous identification of the different ligands and their resulting zirconium complexes throughout this study, we have adopted the nomenclature $^{R_1}PDP^{R_2}$, where R_1 and R_2 represent the forward- and backward-facing substituents, relative to coordination to the metal center, at the 5 and 3 positions of the pyrrole rings, respectively. A small library of novel PDP ligand precursors, H₂^{R₁}PDP^{R₂}, was prepared following the synthetic approaches outlined in Scheme 1. Three new ligand precursors, H₂^{Ph}PDP^{Ph}, H₂^{Me}PDP^H, and H₂^{Me}PDP^{C₆F₅}, were prepared in moderate to good yields following synthetic protocols similar to the ones previously reported for H₂^{Me}PDP^{Ph36} and H₂^{Mes}PDP^{Ph52} using a two-step one-pot approach consisting of a Stetter reaction followed by Paal-Knorr synthesis. 53 This approach relies on the straightforward access to a variety of α,β -unsaturated ketones and allows rigorous control over the positioning of the introduced 3,5-substituents. The synthesis of PDP derivatives with 5H-substitution is not amenable to these

Scheme 2. Synthesis of New $Zr(^{R_1}PDP^{R_2})_2$ Complexes

reaction conditions because of selectivity issues between 2,6-pyridinedicarboxaldehyde and the required α , β -unsaturated aldehyde during the Stetter reaction. Instead, the substituent-free PDP derivative $H_2^{\ H}PDP^H$ was readily obtained via Suzuki–Miyaura coupling of commercially available 2,6-dibromopyridine and N-Boc-2-pyrroleboronic acid followed by thermal deprotection. Finally, PDP derivatives with identical 3,5-pyrrole substituents can be prepared through the condensation of symmetric 1,3-diketones with 2,6-pyridinedimethanamine, as reported by Caulton and coworkers. This method allowed the isolation of $H_2^{\ Me}PDP^{\ Me}$, albeit in poor yield.

Complex Synthesis. Following our previously reported methodology for $Zr(^{Me}PDP^{Ph})_2$, 36 salt metathesis between the lithium salts of the in situ generated, doubly deprotonated ligands, $[^{R_1}PDP^{R_2}]^{2-}$, and 0.5 equiv of $ZrCl_4$ in tetrahydrofuran (THF) furnished $Zr(^{Ph}PDP^{Ph})_2$, $Zr(^{Me}PDP^{H})_2$, $Zr(^{Me}PDP^{E_5})_2$, and $Zr(^{Me}PDP^{Me})_2$ in good yields (Scheme 2). The analogous reaction using $H_2^{H}PDP^{H}$ did not yield $Zr(^{H}PDP^{H})_2$ but instead provided the eight-coordinate complex $Zr(^{H}PDP^{H})_2(THF)_2$. This result presents the first indication that the substituents in the R_1 positions have a significant impact on the coordination geometry and ligand environment around the central zirconium ion because no indication for THF coordination or expansion of the six-coordinate ligand sphere was observed for complexes with 5-pyrrolide substituents. The two THF ligands in Zr-

(${}^{H}PDP^{H})_{2}(THF)_{2}$ proved to be surprisingly labile and were quantitatively removed by repeated coevaporation with aromatic solvents or heating of the complex under a vacuum in the solid state to yield the desired six-coordinate complex $Zr({}^{H}PDP^{H})_{2}$. Alternatively, direct synthetic access to $Zr({}^{H}PDP^{H})_{2}$ in excellent yield is available through the reaction of $H_{2}{}^{H}PDP^{H}$ and 0.5 equiv of tetrabenzylzirconium in benzene. This reaction mirrors our recently developed synthesis for $Zr({}^{Mes}PDP^{Ph})_{2}$ from $H_{2}{}^{Mes}PDP^{Ph}$ and tetrabenzylzirconium at high temperature 38 but proceeds readily at ambient temperature because of the lower steric profile of the ${}^{H}PDP^{H}$ ligand. As expected, the addition of excess THF to $Zr({}^{H}PDP^{H})_{2}$ resulted in the formation of $Zr({}^{H}PDP^{H})_{2}(THF)_{2}$, demonstrating complete reversibility of THF coordination (Scheme 2).

All complexes were characterized by 1 H and 13 C{ 1 H} NMR spectroscopy and exhibit resonances consistent with D_{2d} -symmetric structures and magnetically equivalent PDP ligands on the NMR time scale in solution. This includes the eight-coordinate complex $Zr(^{H}PDP^{H})_{2}(THF)_{2}$, indicating that exchange of the labile THF ligands is rapid on the NMR time scale.

Structural Characterization. All new complexes were characterized by X-ray crystallography (Figure 1) and, with the exception of $Zr(^HPDP^H)_2(THF)_2$, show distorted octahedral coordination environments similar to those reported previously for $Zr(^{Me}PDP^{Ph})_2^{36}$ and $Zr(^{Mes}PDP^{Ph})_2^{38}$. One major distortion of the ZrN_6 core, resulting in symmetry lowering from

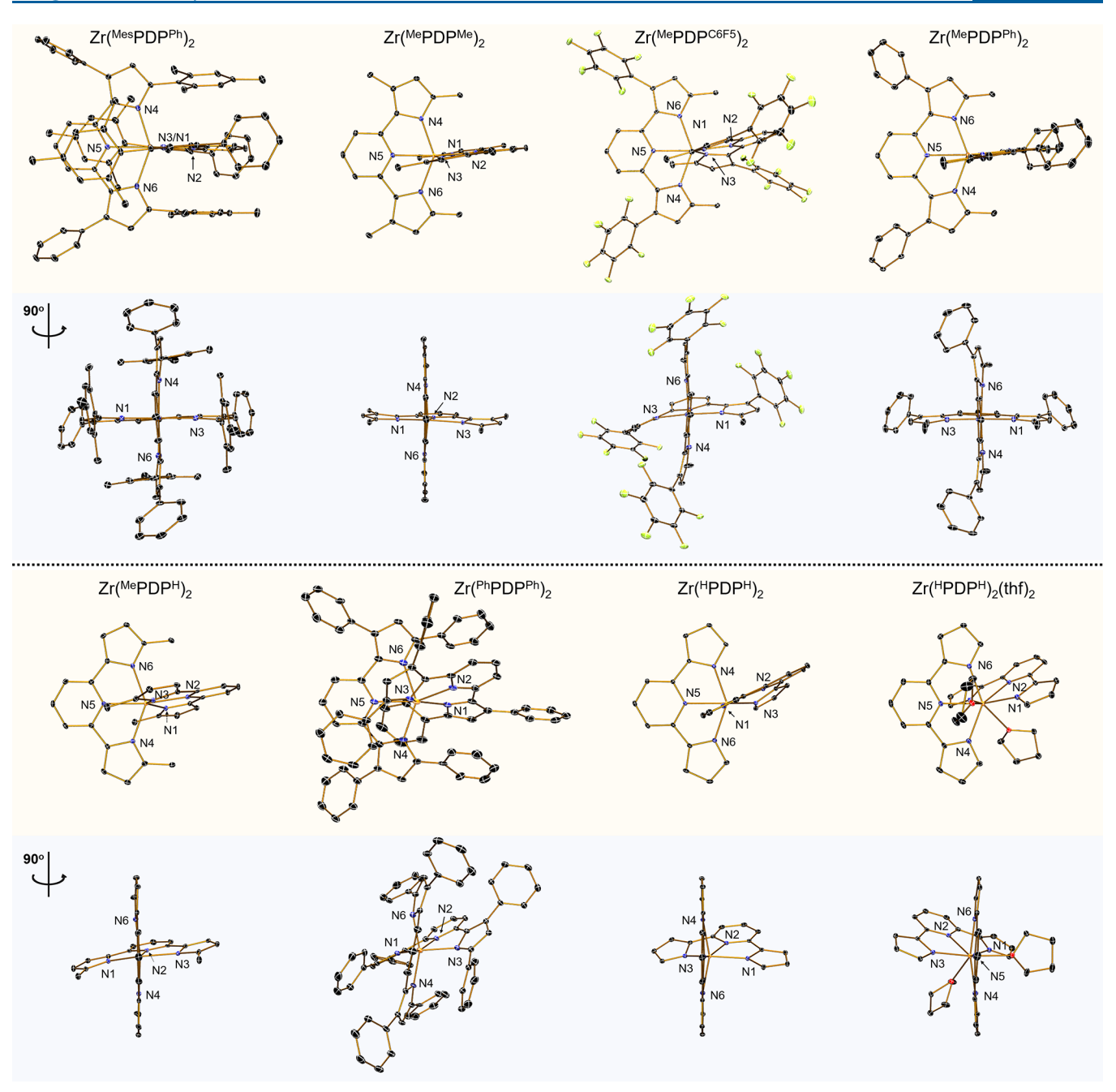


Figure 1. ORTEP representation of the molecular structures of $Zr(^{R_1}PDP^{R_2})_2$ complexes with 30% probability ellipsoids. The structures on the light-blue background are rotated 90° from the structures on the light-orange background. Only one of the two independent molecules in the asymmetric unit of $Zr(^{Me}PDP^{C_6F_5})_2$ is shown. Hydrogen atoms were omitted for clarity.

local O_h to D_{2d} symmetry, is enforced by the limited bite angle of the PDP backbone clearly evidenced by contracted $N_{\rm pyrrolide}$ – $Zr-N_{\rm pyrrolide}$ angles around 140° within each pincer ligand. While the bond lengths for all $Zr(^{R_1}PDP^{R_2})_2$ complexes fall within a relatively narrow range $(Zr-N_{\rm pyridine}=2.28-2.31$ Å; $Zr-N_{\rm pyrrole}=2.14-2.19$ Å), additional deviations from perfect D_{2d} symmetry for the $Zr(PDP)_2$ unit are observed in the solid-state structures of $Zr(^{R_1}PDP^{R_2})_2$ but vary significantly across the series of compounds. The most severe deviations from D_{2d} symmetry for each complex can be quantified by the dihedral angle between the two planes defined by the three nitrogen atoms of each PDP pincer ligand, $\theta_{\rm d}$, and the $N_{\rm pyridine}$ – $Zr-N_{\rm pyridine}$ angle, $\theta_{\rm w}$, with respective dihedral

flattening ($\theta_{\rm d}$ < 90°) and wagging distortions ($\theta_{\rm w}$ < 180°), as shown in Figure 2.

From the $\theta_{\rm d}$ and $\theta_{\rm w}$ angles summarized in Table 1, it is clear that the 5-pyrrolide substituents exert the most significant effect on the extent of solid-state distortion. The sterically demanding 2,4,6-trimethylphenyl (mesityl) substituents in ${\rm Zr}(^{\rm Mes}{\rm PDP}^{\rm Ph})_2$ enforce a rigid structure with near-perfect orthogonal arrangement of the ligands and strict *trans* coordination of the two pyridine rings ($\theta_{\rm d}=89.6^\circ$; $\theta_{\rm w}=179.4^\circ$). The rigidity is further supported by intramolecular, sandwich-type π -stacking interactions between the mesityl substituents of one PDP ligand and the pyridine moiety of the other ($d_{\rm centroid-centroid}\approx 3.6-3.7$ Å). The strong steric protection of the PDP π systems by the mesityl substituents

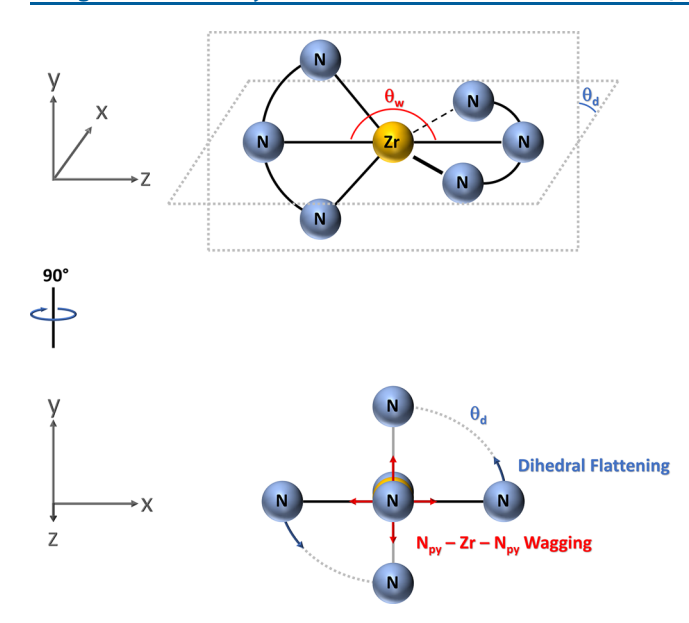


Figure 2. Schematic representation of solid-state distortions for the studied $Zr(^{R_1}PDP^{R_2})_2$ complexes.

Table 1. Comparison of the $\theta_{\rm d}$ and $\theta_{\rm w}$ Angles in the Solid State from X-ray Crystallography

| complex | dihedral angle $\theta_{\rm d}$ $({\rm deg})^a$ | N_{py} – Zr – N_{py} angle θ_w $(deg)^a$ |
|--|---|---|
| $\operatorname{Zr}({}^{\operatorname{Me}}\operatorname{PDP}^{\operatorname{C}_6\operatorname{F}_5})_2$ | 86.2 ^b | 175.0 ^b |
| $\operatorname{Zr}({}^{\operatorname{Me}}\operatorname{PDP}^{\operatorname{Ph}})_2$ | 88.3 | 171.8 |
| $\mathrm{Zr}(^{\mathrm{Me}}\mathrm{PDP}^{\mathrm{H}})_{2}$ | 88.4 | 169.1 |
| $\mathrm{Zr}(^{\mathrm{Me}}\mathrm{PDP}^{\mathrm{Me}})_2$ | 89.6 | 173.1 |
| $\mathrm{Zr}(^{\mathrm{Mes}}\mathrm{PDP}^{\mathrm{Ph}})_2$ | 89.6 | 179.4 |
| $\operatorname{Zr}({}^{\operatorname{Ph}}\operatorname{PDP}^{\operatorname{Ph}})_2$ | 72.9 | 153.8 |
| $Zr(^{H}PDP^{H})_{2}$ | 76.1 | 151.8 |

^aMeasured as shown in Figure 2. ^bAverage value of two independent molecules in the unit cell.

is also responsible for the remarkable stability of Zr- $(^{Mes}PDP^{Ph})_2$, making it the only Zr(PDP) $_2$ derivative discussed in this work that is stable under ambient conditions and does not require rigorously dried solvents for solution experiments. While π -stacking interactions are also observed in Zr- $(^{Ph}PDP^{Ph})_2$, the simple 5-Ph pyrrolide substituents can engage in energetically favored, parallel-displaced π interactions, resulting in a highly distorted molecular structure in the solid state. Notably, one 5-Ph substituent of each PDP ligand engages in π stacking with the pyridine ring of the other PDP unit, while the second 5-Ph substituent can undergo π stacking with one of the pyrrolide moieties because of the reduced steric demand of the ligands.

For the remaining complexes, where no intramolecular π -stacking effects are possible, the presence of S-pyrrolide substituents still has important structural consequences. This is highlighted through a comparison of $Zr(^HPDP^H)_2$ with $Zr(^{Me}PDP^H)_2$. With completely exposed π systems, $Zr(^HPDP^H)_2$ is open to strong intermolecular π stacking (Figure S23), which results in significant distortions of the individual molecules in the crystal lattice ($\theta_d = 76.1^\circ$; $\theta_w = 151.8^\circ$). Because of the steric demands of the 5-methyl substituents, similar distortions are not favorable for $Zr(^{Me}PDP^H)_2$, and hence the complex shows a structure much closer to idealized D_{2d} symmetry ($\theta_d = 88.4^\circ$; $\theta_w = 169.1^\circ$). A further comparison with other 5-methyl-substituted complexes reveals the limited

influence of the 3-pyrrolide substituents on the observed solid-state distortions, with $Zr(^{Me}PDP^{H})_2$, $Zr(^{Me}PDP^{Me})_2$, $Zr(^{Me}PDP^{Ph})_2$, and $Zr(^{Me}PDP^{C6F5})_2$ all exhibiting very similar molecular structures and distortions.

Despite their discussed structural differences in the solid state, it is important to reemphasize that all complexes exhibit time-averaged structures reflecting ideal D_{2d} symmetry on the NMR time scale at room temperature in solution. Because all photophysical, photochemical, and electrochemical experiments described below were conducted in solution, distortions in the solid-state structures are not necessarily representative of the molecular structures under experimental conditions. However, we propose that the solid-state structures are indicative of the overall molecular flexibility, which may influence the accessibility of nonradiative relaxation pathways through vibrational motion in solution and thereby may have profound impacts on the photophysical properties of Zr-(PDP)₂ photosensitizers.

Optical Properties of $Zr(^{R_1}PDP^{R_2})_2$ Complexes. The electronic absorption and emission spectra for all seven $Zr(^{R_1}PDP^{R_2})_2$ complexes in a rigorously dried and deaerated benzene solution at room temperature are shown in Figure 3, and important parameters are summarized in Table 2. For ease

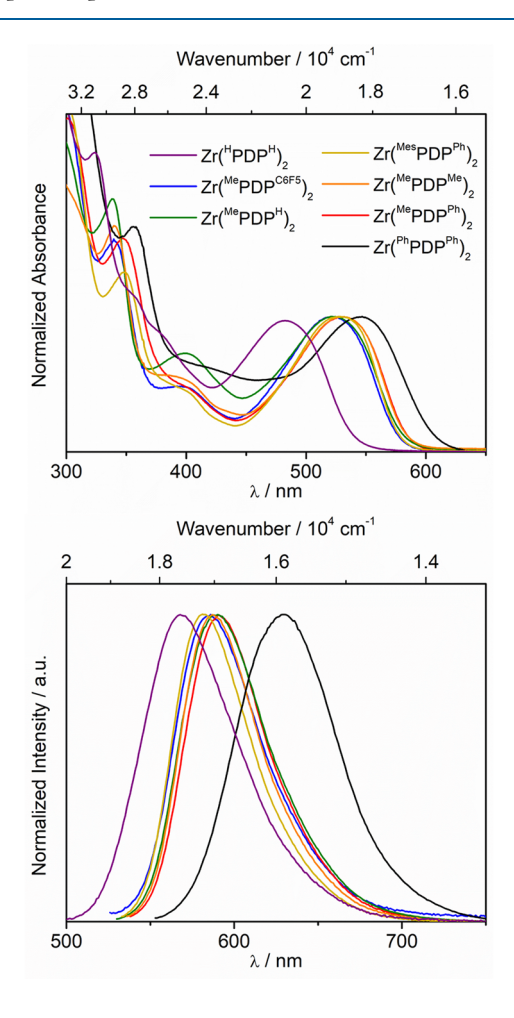


Figure 3. Absorption (top) and emission (bottom; excited at the lowest-energy absorption maxima) spectra of $Zr(^{H}PDP^{H})_2$ (purple), $Zr(^{Me}PDP^{C_eF_5})_2$ (blue), $Zr(^{Me}PDP^{Ph})_2$ (red), $Zr(^{Me}PDP^{H})_2$ (green), $Zr(^{Me}PDP^{Me})_2$ (orange), $Zr(^{Me}PDP^{Ph})_2$ (yellow), and $Zr(^{Ph}PDP^{Ph})_2$ (black) in a benzene solution at room temperature.

Table 2. Comparison of the Optical Properties of $Zr(^{R_1}PDP^{R_2})_2$ Recorded in a Benzene Solution at Room Temperature under an Inert Atmosphere

| complex | $\lambda_{\rm max}({\rm abs})~({\rm nm~cm}^{-1})$ | $\lambda_{\rm max}({\rm em})~({\rm nm}~{\rm cm}^{-1})$ | Stokes shift (cm ⁻¹) | $\tau (\mu s)^a$ | $\Phi_{	ext{PL}}^{b}$ |
|---|---|--|----------------------------------|------------------|-----------------------|
| $\operatorname{Zr}({}^{\operatorname{Me}}\operatorname{PDP}^{\operatorname{C}_6\operatorname{F}_5})_2$ | 521/19190 | 586/17070 | 2129 | 313 | 0.34 |
| $\operatorname{Zr}({}^{\operatorname{Me}}\operatorname{PDP}^{\operatorname{Ph}})_2$ | 532/18800 | 591/16920 | 1877 | 474 | 0.27 |
| $\operatorname{Zr}(^{\operatorname{Me}}\operatorname{PDP}^{\operatorname{H}})_2$ | 524/19080 | 590/16950 | 2135 | 260 | 0.10 |
| $\mathrm{Zr}(^{\mathrm{Me}}\mathrm{PDP}^{\mathrm{Me}})_2$ | 531/18830 | 587/17040 | 1797 | 576 | 0.22 |
| $\mathrm{Zr}(^{\mathrm{Mes}}\mathrm{PDP}^{\mathrm{Ph}})_2$ | 528/18940 | 581/17210 | 1728 | 290 | 0.38 |
| $\operatorname{Zr}({}^{\operatorname{Ph}}\operatorname{PDP}^{\operatorname{Ph}})_2$ | 547/18280 | 629/15900 | 2383 | 190 | 0.11 |
| $\operatorname{Zr}(^{\operatorname{H}}\operatorname{PDP}^{\operatorname{H}})_{2}$ | 482/20750 | 568/17610 | 3141 | 413 | 0.28 |
| $\operatorname{Zr}(^{\operatorname{H}}\operatorname{PDP}^{\operatorname{H}})_{2}(\operatorname{THF})_{2}$ | 430/23360 | 570/17540 | 5812 | 619 | 0.12 |

^aTime-resolved emission data obtained in benzene at room temperature under an inert atmosphere (detection set to emission maximum, 516 nm excitation). ^bMeasured under an inert atmosphere in benzene via the comparative method with Rhodamine 6G as the standard (λ_{exc} = 488 nm; Φ_{PL} = 0.94).

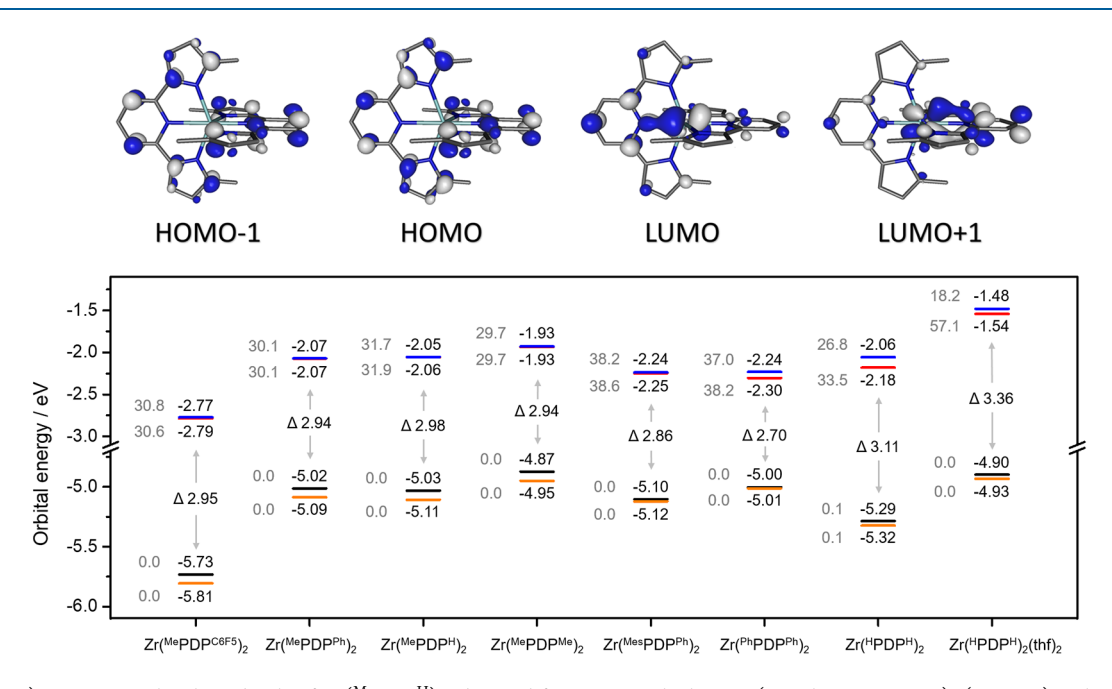


Figure 4. (Top) Frontier molecular orbitals of $Zr(^{Me}PDP^H)_2$ obtained from DFT calculations (isovalue set to 0.05). (Bottom) Calculated frontier molecular orbital energies (eV) for $Zr(^{R_1}PDP^{R_2})_2$. Computed metal contributions (%) are shown in gray to the left of the orbital energies.

of comparison, the absorption spectra were normalized using the intensity of the strongest absorption band in the visible region of each spectrum as the reference. Despite its more limited optical window in the UV region, benzene was chosen over solvents such as THF, acetonitrile, or chlorinated hydrocarbons to prevent solvent coordination and allow a valid comparison between ${\rm Zr}(^{\rm H}{\rm PDP}^{\rm H})_2$ and the remaining six-coordinate species. Aside from ${\rm Zr}(^{\rm H}{\rm PDP}^{\rm H})_2$, the remaining ${\rm Zr}({\rm PDP})_2$ complexes do not show any significant solvato-chromism for absorption or emission.

All seven $Zr(^{R_1}PDP^{R_2})_2$ complexes show qualitatively similar spectra with strong absorption bands in the visible region of the spectrum, which were assigned to transitions with mixed singlet intraligand $(^{1}IL)/^{1}LMCT$ character based on calculations employing time-dependent density functional theory (TD-DFT). As shown previously for $Zr(^{Me}PDP^{Ph})_2$, 37 the donor orbitals for these transitions are exclusively ligand-centered with predominant contributions from the electronrich pyrrolide π systems, while the acceptor orbitals show mixed parentage with major contributions from the metal d_{xz} and d_{yz} orbitals and the pyridine π systems (Figure 4). On the basis of individual calculations for each complex, the amount of

LMCT character varies between 25 and 40% based on the extent of d-orbital contributions to the acceptor orbitals. Among the studied complexes, the two derivatives with aryl substituents in the R_1 position, $Zr(^{Mes}PDP^{Ph})_2$ and $Zr(^{Ph}PDP^{Ph})_2$, exhibit the highest LMCT character at close to 40%, while the remaining complexes show values closer to 30%.

The subset comprised of the four complexes $Zr(^{Me}PDP^{R_2})_2$ ($R_2 = C_6F_5$, Ph, H, Me) allowed a more detailed analysis of the isolated effect of the R_2 substituents on the absorption spectra of $Zr(PDP)_2$ complexes. Despite the markedly different electronic effects of the substituents, from electron-with-drawing (C_6F_5) to electron-donating (Me), the absorption spectra remain remarkably similar, with absorption maxima between 521 and 532 nm (Table 2) and a second band of slightly lower intensity around 400 nm. Considering the more prominent contributions of the pyrrolide π orbitals to the donor [highest occupied molecular orbital (HOMO) and HOMO-1] compared to the acceptor [degenerate lowest unoccupied molecular orbital (LUMO) and LUMO+1] orbitals for the lowest-energy transitions, this observation seemed counterintuitive because a pronounced change in the

energy of the donor relative to the acceptor orbitals due to substituent effects should result in significant shifts in the transition energy and corresponding absorption maximum. Further analysis of the frontier molecular orbitals obtained from DFT calculations showed the expected impact of the R₂ substituents for the predominantly pyrrolide-centered HOMO and HOMO-1. Using $Zr(^{Me}PDP^{H})_{2}$ as the electronically neutral reference point, a stabilizing effect is imparted by the C_6F_5 groups in $Zr(^{Me}PDP^{C_6F_5})_2$, while the Me substituents in Zr(MePDPMe)2 result in a slight destabilization. However, these effects are almost completely compensated for by nearly equivalent changes to the orbital energies of LUMO and LUMO+1, resulting in very similar HOMO/LUMO gaps for all $Zr(^{Me}PDP^{R_2})_2$ complexes (Figure 4). Despite the different contributions from the pyrrolide rings overall, the contributions from the carbon atoms at the 3 position of the heterocycles are nearly identical between HOMO/HOMO-1 and LUMO/LUMO+1. Because the electronic effects of the R_2 substituents on the energy of the PDP π system need to be mediated through the 3 position carrying the different R₂ groups, equal contributions from the carbon atom in this position to the frontier molecular orbitals provide a rationale for the similar changes in both the HOMO/HOMO-1 and LUMO/LUMO+1 energies and, consequently, the small effect of ligand substitution in these positions on the absorption profile.

Substitution in the R₁ positions resulted in more significant changes to the absorption profiles that can be correlated with the electronic properties of R₁. While the Ph substituents in Zr(PhPDPPh)2 are not perfectly coplanar with the pyrrolide rings, partial conjugation extends the π system of the PDP ligand. This results in a stabilization of LUMO/LUMO+1 and a red-shifted absorption profile compared to the Zr(MePDPR2)2 complexes with a low energy maximum at 547 nm. The bulky mesityl substituents in Zr(MesPDPPh)2 remove this conjugation by enforcing a close to perfectly perpendicular arrangement between R_1 = Mes and the pyrrolide rings. As a consequence, the absorption spectra of $Zr(MePDP^{Ph})_2$ and $Zr(MesPDP^{Ph})_2$ are almost identical, indicating similar inductive effects of the electron-donating methyl and electron-rich mesityl groups. Finally, Zr(HPDPH)₂ possesses the most blue-shifted absorption with λ_{max} = 482 nm because of a lack of conjugation from either R₁ or R₂ substituents. The absorption maximum is shifted even further toward higher energy upon coordination of THF and the formation of $\tilde{Z}r(^{H}PDP^{H})_{2}(\tilde{T}HF)_{2}$ ($\lambda_{max} = 430$ nm). This additional blue shift is consistent with the LMCT character of the absorption band because the added THF ligands increase the electron density at the metal center, resulting in less favorable charge transfer to zirconium.

Excitation with UV or visible light with wavelengths shorter than 600 nm [shorter than 550 nm for $Zr(^HPDP^H)_2$] in solution resulted in strong photoluminescence for all complexes. Consistent with the trend observed in the absorption spectra, the four methyl-substituted complexes $Zr(^{Me}PDP^{R_2})_2$ and $Zr(^{Mes}PDP^{Ph})_2$ show very similar emission profiles with maxima in a narrow range of 581–591 nm, while $Zr(^{Ph}PDP^{Ph})_2$ and $Zr(^{H}PDP^{H})_2$ display red- and blue-shifted emission at 629 and 568 nm, respectively. Room-temperature photoluminescence quantum efficiencies were determined by the comparative method S5,56 in deaerated benzene solutions and span a range of $\Phi_{PL} = 0.10-0.38$ (Table 2). Long emission lifetimes of hundreds of microseconds were observed for all compounds under the same conditions ($\tau_{PL} = 190-576~\mu s$;

Table 2). On the basis of our detailed studies of the photophysical properties and excited-state dynamics of $Zr(^{Mes}PDP^{Ph})_2$, 38 this long-lived emission in $Zr(PDP)_2$ complexes at and around room temperature can be assigned to TADF because of a rapid thermal equilibrium between energetically close-lying singlet and triplet excited states. Under these conditions, the observed emission lifetime is a function of multiple factors including the individual lifetimes of the singlet and triplet excited states, S_1 and T_1 , and the energy gap between the two excited states, which is connected to the relative ratio of the forward and reverse intersystem crossing rate constants. Therefore, a straightforward correlation of the lifetimes and quantum yields with other molecular properties is difficult and beyond the scope of this work.

An interesting case is presented by the closely related six-and eight-coordinate complexes $Zr(^HPDP^H)_2$ and $Zr(^HPDP^H)_2(THF)_2$. Despite the substantial differences in their absorption spectra, the emission profiles of $Zr(^HPDP^H)_2$ in benzene and $Zr(^HPDP^H)_2(THF)_2$ in THF are nearly identical, resulting in a larger Stokes shift for the eight-coordinate complex (Figure 5). On the one hand, this increase in the

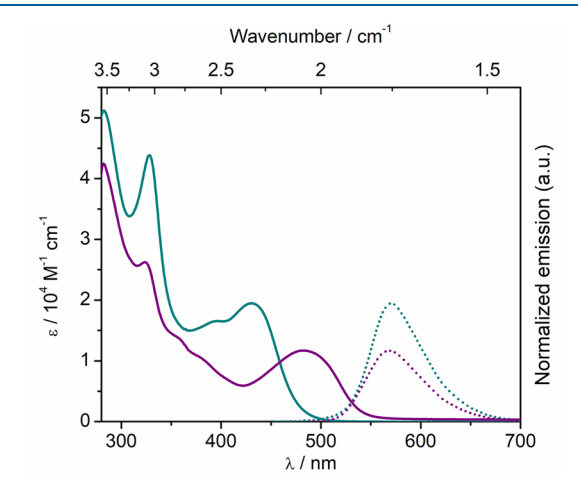


Figure 5. Absorption (solid line) and emission (dotted line; excited at the lowest-energy absorption maxima) spectra of $Zr(^HPDP^H)_2$ (purple) in a benzene solution and $Zr(^HPDP^H)_2(THF)_2$ (dark cyan) in a THF solution at room temperature.

Stokes shift may simply be the result of more pronounced geometry changes between the ground and excited states for Zr(HPDPH)2(THF)2, leading to increased energy loss through internal conversion. Potential ligand dissociation and equilibria between different $Zr(^{H}PDP^{H})_{2}(THF)_{n}$ (n = 0-2) species in solution could amplify these processes. On the other hand, the larger energy gap between absorption and emission for the eight-coordinate complex could also indicate changes in the primary nature of the emission between Zr(HPDPH)2 and Zr(HPDPH)2(THF)2. It is reasonable to assume that the primary emission mechanism in the six-coordinate complex Zr(HPDPH)₂ is TADF, but the situation is less clear for Zr(HPDPH)2(THF)2. A plausible hypothesis for the observed changes in the photophysical properties of Zr-(HPDPH)2(THF)2 is direct emission from the lowest-energy triplet state via phosphorescence. The difference in the Stokes shift of 2671 cm⁻¹ between the six- and eight-coordinate complexes is on the same order of magnitude as the singlettriplet energy gap, $\Delta E_{S_1-T_1} = 1650$ cm⁻¹, observed

experimentally for $\rm Zr(^{Mes}PDP^{Ph})_2$. This explanation is also consistent with the lifetime and quantum yield data. Zr-($^{\rm H}PDP^{\rm H})_2(\rm THF)_2$ shows a significantly longer emission lifetime (619 vs 413 μs) with a lower photoluminescence quantum yield (0.12 vs 0.28), indicating very similar rates of nonradiative excited-state deactivation (1422 vs 1744 s⁻¹) but a change by a factor of more than 3 in the radiative decay rates (194 vs 678 s⁻¹). Experimental validation of this hypothesis through temperature-dependent emission studies is beyond the scope of this work but will be attempted in future studies.

Beyond the analysis of electronic substituent effects on the optical properties, we were interested in investigating potential correlations between the structural differences observed in the solid state and the solution luminescence properties of $Zr(R_1PDP_2)_2$. On the basis of the optical properties summarized in Table 2, neither the photoluminescence quantum yield nor the emission lifetime shows a clear correlation with the observed structural distortions. This is not surprising given that, for emission via TADF, both parameters depend on a complex interplay of fundamental processes including internal conversion, (reverse) intersystem crossing, and nonradiative relaxation of the multiple excited states involved. However, there is a clear correlation between the observed Stokes shift between absorption and emission maxima and the extent of molecular distortion in the solid state. The $Zr(^{R_1}PDP^{R_2})_2$ derivatives that experience the smallest distortions in their solid-state structures exhibit the smallest Stokes shifts (Figure 6). This is consistent with a smaller structural reorganization for more rigid Zr(PDP), complexes after photoexcitation and a reduced energy loss through vibrational relaxation in the excited state. One notable outlier is $Zr(^{Ph}PDP^{Ph})_2$, for which the Stokes shift is significantly smaller than expected based on its highly distorted solid-state structure. This can most likely be attributed to a weakening of the intramolecular π -stacking interactions in aromatic solvents, which may result in a more symmetric structure in solution compared to the solid state.

Electrochemistry and Excited-State Redox Potentials. Cyclic voltammograms (CVs) were recorded in solutions containing 0.1 M $[N(n-Bu)_4]PF_6$ as the supporting electrolyte by using a glassy-carbon working electrode. Ferrocene was used as an internal standard, and all potentials are references against the ferrocenium/ferrocene (Fc⁺/Fc) couple. Figure 7 shows the CVs of the seven six-coordinate complexes Zr(R₁PDP^{R₂}), and Zr(HPDPH)₂(THF)₂. The extracted redox potentials are summarized in Table 3. To allow for solvent stability under highly reducing conditions, CVs were recorded in a THF solution. As the only exception, the CV of Zr(HPDPH), was recorded in 1,2-difluorobenzene to avoid solvent coordination and maintain the six-coordinate species in solution. To establish comparability between the potentials recorded in THF and 1,2-difluorobenzene, the redox properties for Zr(MePDPPh)2 were measured in both solvents and show excellent agreement between experiments. Unfortunately, the smaller solvent window for 1,2-difluorobenzene prevented detection of the third reduction event for Zr(MePDPPh)2 reported previously³⁶ and any potential reductions beyond -3.0 V for Zr(HPDPH)₂.

With the exception of $Zr(^{Me}PDP^{C_6F_5})_2$, all complexes show at least two fully reversible redox events corresponding to two consecutive single-electron reductions. The absence of a second reversible reduction and the quasi-reversible nature of even the first reduction in $Zr(^{Me}PDP^{C_6F_5})_2$ are likely due to the

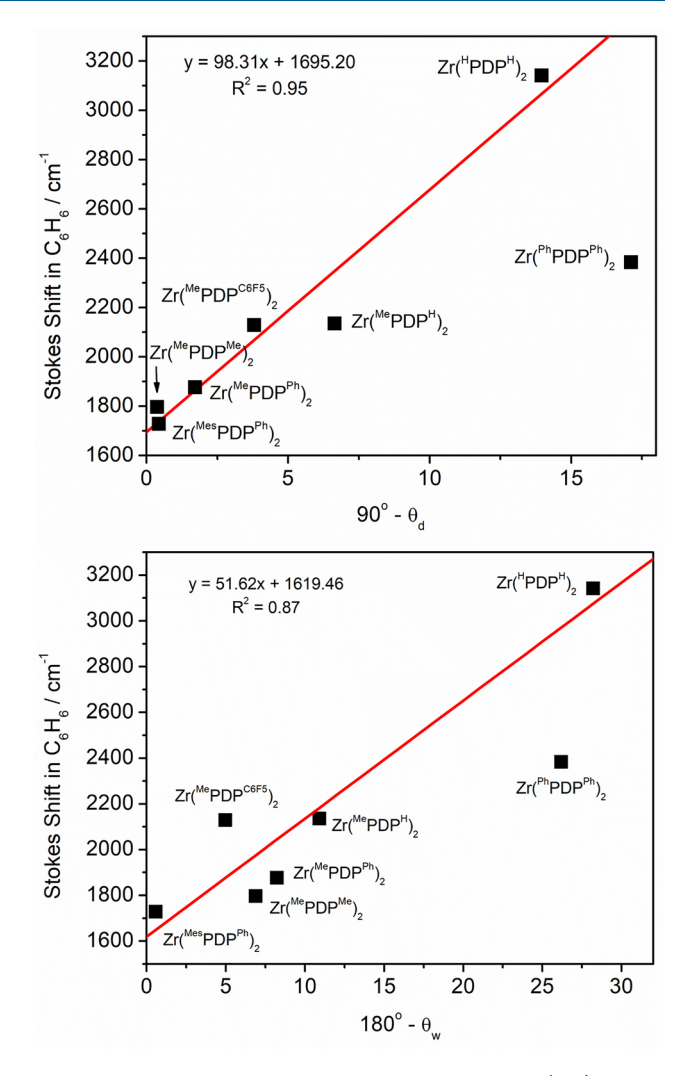


Figure 6. Correlation between θ_d and the Stokes shifts (top) and θ_w and the Stokes shifts (bottom). For reasons discussed in the main text, $Zr^{Ph}PDP^{Ph}_2$ was excluded from the fit.

presence of electron-poor pentafluorophenyl substituents that are not stable under the highly reducing conditions. The reduction potentials within the four-membered series Zr-(MePDPR₂)₂ are strongly influenced by the nature of the R₂ substituents with more positive redox potentials for the electron-withdrawing groups (C₆F₅ and Ph) and more negative potentials for the electron-donating Me substituents in Zr(MePDPMe)₂. Over the complete series of Zr(MePDPR₂)₂, the potentials for the first reduction cover a range of nearly 600 mV, highlighting the tunability of the electrochemical properties by means of the R2 substituents. In a similar fashion, the methyl substituents on the R₁ aryl substituents in Zr-(MesPDPPh)2 shift the reduction to more negative potentials compared to Zr(PhPDPPh)₂. The observation that both R₁ and R₂ substituents have an effect on the ground-state redox properties is consistent with the composition of the LUMO of the Zr(PDP)₂ motif, which shows significant contributions of the carbon atoms at the 3 and 5 positions of the pyrrolide moieties (Figure 4).

For complexes with the lowest second reduction potentials, $Zr(^{Me}PDP^{Ph})_2$ and $Zr(^{Ph}PDP^{Ph})_2$, a third reversible reduction event could be detected at potentials beyond -3.1~V in THF. The remarkable range of accessible redox states for [Zr-

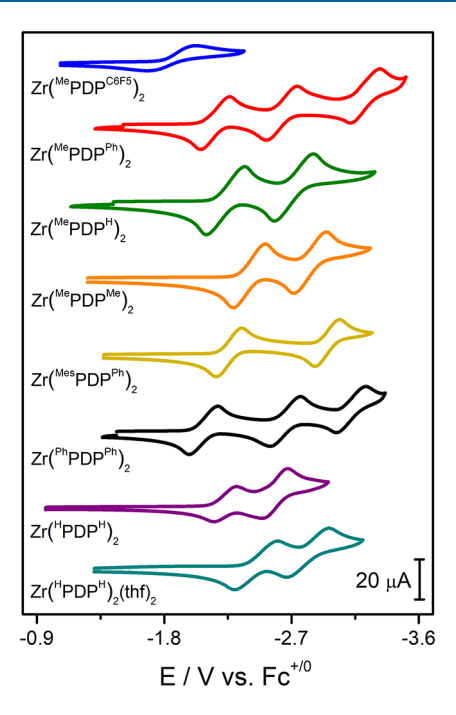


Figure 7. CVs of $Zr(^{Me}PDP^{C_6F_5})_2$ (blue), $Zr(^{Me}PDP^{Ph})_2$ (red), $Zr(^{Me}PDP^H)_2$ (green), $Zr(^{Me}PDP^{Me})_2$ (orange), $Zr(^{Mes}PDP^{Ph})_2$ (yellow), $Zr(^{Ph}PDP^{Ph})_2$ (black), and $Zr(^{H}PDP^{H})_2(THF)_2$ (dark cyan) in THF and $Zr(^{H}PDP^{H})_2$ (purple) in 1,2-difluorobenzene at room temperature (scan rate 200 mV s⁻¹; 0.1 M [N(n-Bu) $_4$]PF $_6$; glassy-carbon working electrode).

Table 3. Redox Potentials for $Zr(^{R_1}PDP^{R_2})_2$ and $Zr(^{H}PDP^{H})_2(THF)_2$

| complex | $E_{1/2}(0/1-)$ (V) ^a | $E_{1/2}(1-/2-)$ (V) ^a | $E_{1/2}(2-/3-)$ $(V)^a$ |
|--|----------------------------------|-----------------------------------|--------------------------|
| $\operatorname{Zr}({}^{\operatorname{Me}}\operatorname{PDP}^{\operatorname{C}_{\operatorname{e}}\operatorname{F}_{\operatorname{s}}})_{2}$ | -1.85^{b} | | |
| $\operatorname{Zr}({}^{\operatorname{Me}}\operatorname{PDP}^{\operatorname{Ph}})_2$ | -2.16^{c} (-2.14^{d}) | -2.63^{c} (-2.57^{d}) | $-3.22^{c,e}$ |
| $\operatorname{Zr}(^{\operatorname{Me}}\operatorname{PDP}^{\operatorname{H}})_{2}$ | -2.21 | -2.70 | |
| $\operatorname{Zr}(^{\operatorname{Me}}\operatorname{PDP}^{\operatorname{Me}})_2$ | -2.42 | -2.85 | |
| $\operatorname{Zr}(^{\operatorname{Mes}}\operatorname{PDP}^{\operatorname{Ph}})_2$ | -2.25^{f} | -2.95^{f} | |
| $\operatorname{Zr}(^{\operatorname{Ph}}\operatorname{PDP}^{\operatorname{Ph}})_2$ | -2.09 | -2.67 | -3.13 |
| $Zr(^{H}PDP^{H})_{2}$ | -2.24^{d} | -2.56^{d} | /e |
| $Zr(^{H}PDP^{H})_{2}(THF)_{2}$ | -2.45 | -2.82 | |

 a All potentials are referenced against the Fc⁺/Fc redox couple. b Quasi-reversible. c From ref 36. d Potentials measured in 1,2-difluorobenzene. e The 1,2-difluorobenzene solvent window is not wide enough to observe the third reduction event ($E_{\rm max}\approx-3.0~{\rm V}$). f From ref 38.

 $(PDP)_2]^n$ complexes under reducing conditions can be traced to the redox activity of the PDP ligands. Each of the central pyridine rings of the two PDP ligands can accept one electron, as was demonstrated for the redox series $[Cr(^{Me}PDP^{Ph})_2]^{n-}$ (n=1,2, or 3), in which all members contain a chromium(III) ion. As reported previously, $Zr(^{Me}PDP^{Ph})_2$ exhibits unique redox properties compared to the other complexes discussed in this work with two additional redox events that can be attributed to single-electron oxidations. As expected for a zirconium(IV) species, these oxidations are exclusively ligand-centered and are made possible by the increased steric protection of the PDP π system provided by the mesityl substituents.

With ground-state reduction potentials, $E_{1/2}(0/1-)$, and emission energies, $E_{0,0}$, in hand, estimates for the potentials of single-electron reduction of Zr(R1PDPR2)2 complexes in the excited state, $E_{1/2}(0^*/1-)$, were calculated as $E_{1/2}(0^*/1-) =$ $E_{1/2}(0/1-) + E_{0,0}$. One caveat of this approach is determination of the excited-state energy, $E_{0,0}$, from λ_{max} of the emission band: Because the emission in Zr(PDP)₂ complexes is due to TADF rather than phosphorescence, the observed emission spectrum at room temperature reflects an approximation of the S₁ excited-state energy. However, excited-state electron transfer is more likely to occur from the long-lived T₁ state due to its higher thermal population established via rapid S_1/T_1 equilibrium following photo-excitation. For $Zr(^{Mes}PDP^{Ph})_2$, the only complex for which the triplet energy was determined via the detection of a phosphorescence band by low-temperature emission spectroscopy, 38 this distinction amounts to a difference in $E_{0,0}$ and the resulting excited-state potential of approximately 0.2 eV. Nevertheless, the estimated excited-state potentials using the room temperature TADF emission maximum are useful indicators for the feasibility of photoinduced single-electron transfer during photocatalysis, in our experience. For example, the excited state of $Zr(^{Mes}PDP^{Ph})_2$ is reductively quenched by 1,3-dimethyl-2-phenyl-2,3-dihydro-1*H*-7-methoxybenzo[*d*]imidazole ($^{\text{MeO}}$ BIH), which possesses a reported redox potential of -0.22 V. Using the phosphorescence energy of Zr(MesPDP^{Ph})₂, the excited-state redox potential of the complex can be estimated as -0.31 V, which indicates that excited-state reduction by $^{\text{MeO}}\text{BIH}$ is thermodynamically disfavored. In contrast, using the TADF emission maximum, a potential of -0.12 V is obtained, which suggests favorable excited-state electron transfer in agreement with the experimental data. Bearing this in mind, the $E_{0.0}$ values reported in Table 4 were derived from λ_{max} of the room-temperature emission spectra.

Table 4. Excited-State Potentials for Zr(R1PDPR2),

| complex | $E_{1/2}(0/1-)$ (V, vs $Fc^{+/0}$) | $(eV)^a$ | $E_{1/2}(0*/1-)_b(V, vs Fc^{+/0})^b$ |
|--|-------------------------------------|----------|--------------------------------------|
| $\operatorname{Zr}({}^{\operatorname{Me}}\operatorname{PDP}^{\operatorname{C}_6\operatorname{F}_5})_2$ | -1.85° | 2.12 | +0.27 |
| $\operatorname{Zr}({}^{\operatorname{Me}}\operatorname{PDP}^{\operatorname{Ph}})_2^{d}$ | -2.16 | 2.10 | -0.06 |
| $\operatorname{Zr}(^{\operatorname{Me}}\operatorname{PDP}^{\operatorname{H}})_2$ | -2.21 | 2.10 | -0.11 |
| $\mathrm{Zr}(^{\mathrm{Me}}\mathrm{PDP}^{\mathrm{Me}})_2$ | -2.42 | 2.11 | -0.31 |
| $\operatorname{Zr}({}^{\operatorname{Mes}}\operatorname{PDP}^{\operatorname{Ph}})_2^{e}$ | -2.25 | 2.13 | -0.12 |
| $\operatorname{Zr}({}^{\operatorname{Ph}}\operatorname{PDP}^{\operatorname{Ph}})_2$ | -2.09 | 1.97 | -0.12 |
| $Zr(^{H}PDP^{H})_{2}$ | -2.24 | 2.18 | -0.06 |

^aApproximated as the emission energy at room temperature. ^bCalculated using $E_{1/2}(0^*/1-) = E_{1/2}(0/1-) + E_{0,0}$. ^cQuasi-reversible redox event. ^dFrom ref 36. ^eFrom ref 38.

As in the case of the optical properties and ground-state redox potentials, the clearest trend for the excited-state redox properties can be observed within the series $Zr(^{\text{Me}}PDP^{R_2})_2$. Because the R_2 substituents strongly affect $E_{1/2}(0/1-)$ but have no significant influence on $E_{0,0}$, any changes to the ground-state redox properties directly propagate to the excited-state redox potential $E_{1/2}(0^*/1-)$. This allows the straightforward tuning of $E_{1/2}(0^*/1-)$ over nearly 600 mV (-0.31 to +0.27 V), with only minor changes in the absorption or emission profiles. In contrast, changes in R_1 affect both the redox properties and excited-state energies. For the complexes studied in this work, the two effects counterbalance almost

Inorganic Chemistry Forum Article pubs.acs.org/IC

completely because more negative reduction potentials are associated with more blue-shifted emission bands, i.e., higher $E_{0,0}$ values. Consequently, the excited-state potentials of the four complexes $Zr(^{Ph}PDP^{Ph})_2$, $Zr(^{Mes}PDP^{Ph})_2$, $Zr(^{H}PDP^{H})_2$, and Zr(MePDPPh), cover a relatively narrow potential range of only 60 mV (-0.06 to -0.12 V).

Photoinduced Single-Electron Transfer. With excitedstate potentials of +0.27 to -0.31 V, Zr(R1PDPR2), photosensitizers should be considered to be mild oxidants in their excited state and require relatively strong sacrificial reductants to participate in excited-state electron transfer. We previously identified benzimidazolium hydride (RBIH) derivatives as suitable electron donors that can quench the excited state of Zr(MePDPPh)₂ through photoinduced single-electron transfer.³⁶ One key piece of evidence supporting excited-state electron transfer in these studies was the strong dependence of the quenching rate constant on the redox potential of the RBIH derivative,³⁷ which can be conveniently controlled through the choice of substituent on the benzimidazolium fragment. 58 With a series of Zr(MePDPR2)2 complexes covering a range of excited-state redox potentials in hand, we conducted the reverse experiment, in which the potential of the sacrificial reductant was kept constant. To ensure sufficient reducing power even for Zr(MePDPMe)2, which exhibits the most negative excited-state potential of -0.31 V, 1,3-dimethyl-2-(2,4,6-trimethoxyphenyl)-2,3-dihydro-1*H*-benzo[*d*]imidazole $(MeO)_3PhBIH$; $E_{ox} = -0.33 \text{ V}$) was identified as a suitable quencher. The resulting Stern–Volmer plots for $Zr(^{Me}PDP^{R_2})_2$ $(R_2 = Me, H, Ph, C_6F_5)$ are shown in Figure 8 and exhibit a

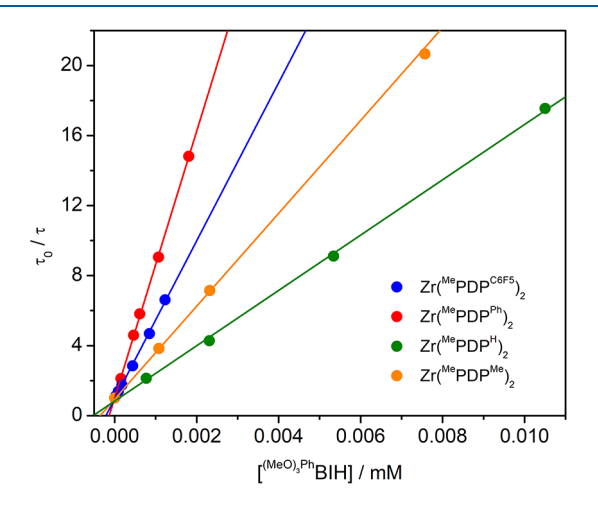


Figure 8. Stern-Volmer plots obtained via time-resolved emission spectroscopy.

strictly linear dependence of the luminescence lifetime on the concentration of (MeO)₃PhBIH. This behavior is indicative of a diffusion-controlled dynamic quenching process, and the corresponding Stern-Volmer constants, K_{SV}, and quenching rate constants, k_q , are summarized in Table 5. As expected for quenching via electron transfer, the values for k_q are correlated to the excited-state redox potentials of the Zr(MePDPR2)2 photosensitizer.

Following excited-state electron transfer with $^{(MeO)_3Ph}BIH$, the electron-rich photosensitizer Zr(MePDPMe)₂ produces the most powerful ground-state reductant of any Zr(PDP)2 complex reported to date. Given the negative potential of $E_{1/2}([\mathrm{Zr}(^{\mathrm{Me}}\mathrm{PDP}^{\mathrm{Me}})_2]^{0/1-}) = -2.42 \text{ V vs } \mathrm{Fc}^+/\mathrm{Fc}, \text{ we were}$

Table 5. Stern-Volmer Constants and Quenching Rate Constants for Zr(MePDPR2),

| complex | $K_{\rm SV}~({\rm L~mol^{-1}})$ | $k_{\rm q}(\times 10^8 \ { m L \ mol^{-1} \ s^{-1}})$ | $E_{1/2}(0*/1-)$ (V, vs Fc ^{+/0}) |
|--|---------------------------------|---|---|
| $\operatorname{Zr}({}^{\operatorname{Me}}\operatorname{PDP}^{\operatorname{C}_6\operatorname{F}_5})_2$ | 446000 ± 5300 | 31.0 | +0.27 |
| $\operatorname{Zr}({}^{\operatorname{Me}}\operatorname{PDP}^{\operatorname{Ph}})_2$ | 763000 ± 3800 | 23.5 | -0.06 |
| $\mathrm{Zr}(^{\mathrm{Me}}\mathrm{PDP}^{\mathrm{H}})_{2}$ | 158000 ± 1600 | 11.5 | -0.11 |
| $\operatorname{Zr}(^{\operatorname{Me}}\operatorname{PDP}^{\operatorname{Me}})_2$ | 265000 ± 1500 | 4.9 | -0.31 |

interested in testing the scope of potential substrates for reductive photoredox catalysis. With few exceptions, previous examples for photoredox catalysis using zirconium photosensitizers relied on the use of activated alkyl halides or olefins, which are relatively easy targets for photochemical reduction. In contrast, aryl halides are generally considered more challenging substrates, 59 with the reactivity decreasing from aryl iodides to the more readily available aryl chlorides. 60 first proof of principle, dehalogenation of methyl 4iodobenzoate was attempted using $Zr(^{Me}PDP^{Me})_2$ as the photocatalyst (10 mol %) and $^{(MeO)_3Ph}BIH$ as the sacrificial reductant and hydrogen-atom donor. Following irradiation with green light (light-emitting diode; $\lambda_{max} = 520$ nm) for 14 h, the desired product, methyl benzoate, was obtained in good yield with nearly quantitative conversion of the starting material (Scheme 3). Independent control experiments in the absence of light or photosensitizer resulted in quantitative recovery of the starting material, highlighting the photochemical nature of the reaction. When the electron-withdrawing methyl carboxylate substituent was replaced with bromide, dehalogenation of 4-bromo-1-iodobenzene using 1 equiv of (MeO)₃PhBIH furnished bromobenzene in good yield, demonstrating excellent selectivity for reduction of the more reactive aryl iodide. However, significantly extended irradiation times were required compared to those of dehalogenation of the more activated methyl iodobenzoate. The addition of excess (MeO)₃PhBIH resulted in the partial reduction of bromobenzene, indicating that the photocatalyst is able to engage aryl bromide substrates albeit with reduced efficiency. Finally, the electron-donating methoxy group in 4-iodoanisole resulted in a further reduction in reactivity and incomplete conversion to anisole even after nearly 3 days of irradiation. Nevertheless, the successful activation of an electron-rich benzene derivative encouraged further experiments with more challenging aryl chlorides.

Starting again with electron-poor substrates, methyl 4chlorobenzoate was readily reduced to methylbenzoate using $Zr(^{Me}PDP^{Me})_2$ in combination with $^{(MeO)_3Ph}BIH$. Notably, no significant difference in the reaction times or yields was found between the iodo- and chlorobenzoate substrates. The dehalogenation reactivity with aryl chlorides was readily extended to 4-chlorobenzonitrile as a second electron-poor aryl halide but required a substantial increase in the irradiation time to 24 h. Unfortunately, switching to less reactive aryl chloride derivatives such as 1,2- or 1,3-dichlorobenzene resulted in dramatically reduced conversions even after extended irradiation times of up to 7 days. Despite the limited substrate scope presented here, our studies provide the first example for photochemical activation of aryl chlorides using a zirconium photosensitizer. Importantly, our photocatalytic system is driven by relatively low-energy green light and does not need electrochemical activation to access the highly reducing potentials required. This demonstrates the potential

Scheme 3. Aryl Halide Dehalogenation Reactions Using Zr(MePDPMe), as the Photocatalyst

for further applications of $Zr(PDP)_2$ chromophores in photochemical transformations requiring strongly reducing conditions.

CONCLUSIONS

A family of seven photoluminescent bis(pyridinedipyrrolide)zirconium complexes has been synthesized and investigated by X-ray crystallography, electronic absorption and emission spectroscopy, and cyclic voltammetry. The substituents at the 3 and 5 positions of the pyrrolide moieties have distinct effects on the photosensitizer characteristics of these Zr- $(^{R_1}PDP^{R_2})_2$ compounds. The steric profile of the forward-facing R₁ substituents, corresponding to the 5-pyrrolide substituents, exerts a major influence on the molecular structure and the overall stability of the complexes. This is reflected in the exceptional air and water stabilities of Zr(MesPDPPh)2 compared to those of the remaining $Zr(^{R_1}PDP^{R_2})_2$ complexes and the facile formation of eight-coordinate Zr-(HPDPH)2(THF)2 from Zr(HPDPH)2, which is unique among the reported Zr(PDP)₂ complexes. Additionally, the absorption and emission profiles as well as the electrochemical properties of the complexes are sensitive to the nature of the R₁ substituents, indicating significant electronic effects through extension of the ligand π system by conjugation. In contrast, the backward-facing R₂ substituents at the 3 position of the pyrrolide units contribute exclusively through electronic effects and have negligible contributions to the structural properties of the Zr(PDP)₂ core. Most importantly, changes to the R₂ substituents substantially impact the electrochemical properties of the complexes, while the optical properties remain almost unchanged. The small influence on the absorption and emission profiles can be rationalized through similar effects of the R₂ substituents on the energies of the filled and empty frontier molecular orbitals. As a consequence, manipulation of the R2 substituents allows convenient tuning of the groundand excited-state redox properties of $Zr(^{R_1}PDP^{R_2})_2$ complexes independent of the absorption and emission energies. All seven complexes produce powerful ground-state reductants following excited-state electron transfer with RBIH derivatives through reductive quenching. The most reducing complex, Zr-(MePDPMe)₂, was evaluated for its photochemical reactivity toward aryl iodides and more challenging aryl chloride substrates. The observed dehalogenation reactions represent the first examples for photochemical aryl halide activation with group 4 photosensitizers and provide sufficient proof of concept for the further exploration of early-transition-metal chromophores in challenging photocatalytic transformations under mild conditions.

EXPERIMENTAL DETAILS

General Considerations. All air- and moisture-sensitive manipulations were carried out using standard high-vacuum-line, Schlenk, or cannula techniques or in an MBraun inert-atmosphere drybox containing an atmosphere of purified nitrogen. Solvents for air- and moisture-sensitive manipulations were dried and deoxygenated using a Glass Contour Solvent Purification System and stored over 4 Å molecular sieves. Deuterated solvents for NMR spectroscopy were purchased from Cambridge Isotope Laboratories and distilled from sodium metal (C₆D₆), 4 Å molecular sieves (CD₃CN), or CaH₂ (CDCl₃). Tetrabenzylzirconium, 61,62 Zr(MePDPPh)₂,36 and Zr- ${\rm ^{
m Mes}PDP^{
m Ph})_2}^{
m 38}$ were prepared following literature procedures. All remaining chemicals were purchased from commercial sources (Fisher Scientific, VWR, and Sigma-Aldrich) and used without further purification. All solids were dried under high vacuum, and lowboiling liquids were dried over CaH2 and vacuum-transferred into oven-dried glassware in order to bring them into the glovebox. Highboiling liquid substrates were degassed, dried over CaH2, and filtered through Celite in the glovebox.

Physical Measurements. ¹H and ¹³C{¹H} NMR spectra were recorded on an Agilent 400 MHz spectrometer, a JEOL 400 MHz YH spectrometer, or a Varian INOVA 600 MHz spectrometer. All chemical shifts are reported relative to SiMe₄ using ¹H (residual) chemical shifts of the solvent as a secondary standard. Electronic spectra were recorded using a Shimadzu UV-1800 spectrophotometer in gastight quartz cuvettes with 10 mm path length and fitted with J-Young valves. Emission spectra were obtained in 10-mm-path-length gastight quartz cuvettes with J-Young valves using a Shimadzu RF-5301 PC spectrofluorophotometer. Photoluminescent decay data were collected using a Horiba Jobin-Yvon Fluorolog-3 spectrofluorometer with a single-photon-counting module in multichannel scaler mode and a 516 nm SpectraLED pulsed excitation source. Lifetimes were determined through exponential fitting using the provided decay analysis software package, DAS v6.1. Cyclic voltammetry measurements were conducted under a nitrogen atmosphere inside a MBraun drybox using a Gamry Interface 1000 electrochemical workstation in a single-compartment cell using 1 mM sample solutions with 0.1 M tetrabutylammonium hexafluorophosphate as the supporting electrolyte. A three-electrode setup was employed with glassy carbon electrode as the working electrode, a platinum sheet as the counter electrode, and a silver wire as the quasi-reference electrode. Ferrocene (Fc) was added as an internal standard after completion of the measurements, and all potentials were referenced versus the Fc⁺/Fc couple. High-resolution mass spectrometry (HRMS) spectra were obtained on a Thermo Finnigan Linear Trapping Quadrupole mass

spectrometer. Elemental analyses were performed at Robertson Microlit Laboratories, Inc., in Ledgewood, NI.

2,6-Bis(3,5-diphenyl-1H-pyrrol-2-yl)pyridine $(H_2^{Ph}PDP^{Ph})$. The synthesis was carried out according to a modified literature procedure. 36,52 2,6-Pyridinedicarboxaldehyde (2.00 g, 14.80 mmol, 1.00 equiv), 1,3-diphenylprop-2-en-1-one (6.17 g, 29.60 mmol, 2.00 equiv), and 3-benzyl-5-(2-hydroxyethyl)-4-methylthiazolium chloride (2.395 g, 8.88 mmol, 0.6 equiv) were mixed in a 250 mL Schlenk flask under an argon atmosphere. Absolute ethanol was added, and the mixture was heated to reflux. A solution of sodium tert-butoxide (853 mg, 8.88 mmol, 0.6 equiv) in ethanol was added via a syringe, and heating was continued for 24 h. The reaction was cooled to room temperature, and ammonium acetate (6.85 g, 88.81 mmol, 6.00 equiv) was added to the mixture. The reaction mixture was heated to reflux open to air for 24 h. The solid precipitate was collected via filtration, washed with cold ethanol, and dried under high vacuum to yield the desired product as a pale-yellow solid. Yield: 6.018 g, 79%. Mp: 231–233 °C. ¹H NMR (400 MHz, C_6D_6): δ 9.50 (s, 2H, NH), 7.59 (d, I = 7.2 Hz, 4H, PhH), 7.32 (d, I = 7.6 Hz, 4H, PhH), 7.24 (t, I = 7.6 Hz, 4H, PhH), 7.18-7.10 (m, 8H, PyH and PhH), 7.05 (t, I = 1.00 (m, 8H, PyH and PhH)7.2 Hz, 2H, PhH), 6.72 (d, J = 8.0 Hz, 1H, p-PyH), 6.68 (d, J = 2.4 Hz, 2H, PyH). 13 C NMR (101 MHz, C_6D_6): δ 150.83, 137.75, 136.65, 133.39, 132.41, 129.76, 129.20, 128.92, 128.15 127.55, 127.12, 126.88, 124.48, 117.89, 110.89. HRMS (ESI). Calcd for $C_{37}H_{28}N_3^+$ ([M + H]⁺): m/z 514.22777. Found: m/z 514.22885.

2,6-Bis(5-methyl-1H-pyrrol-2-yl)pyridine (H₂MePDPH). The synthesis was carried out according to a modified literature procedure.^{36,52} 2,6-Pyridinedicarboxaldehyde (2.00 g, 14.80 mmol, 1.00 equiv), methyl vinyl ketone (2.59 g, 37.00 mmol, 2.50 equiv), and 3-benzyl-5-(2-hydroxyethyl)-4-methylthiazolium chloride (2.395 g, 8.88 mmol, 0.6 equiv) were mixed in a 250 mL Schlenk flask under an argon atmosphere. Absolute ethanol was added, and the mixture was heated to reflux. A solution of sodium tert-butoxide (853 mg, 8.88 mmol, 0.6 equiv) in ethanol was added via a syringe, and heating was continued for 24 h. The reaction was cooled to room temperature, and ammonium acetate (11.41 g, 148.02 mmol, 10.00 equiv) was added to the mixture. The reaction mixture was heated to reflux open to air. After 24 h, the solvent was removed. The resultant was diluted with H2O, and the crude product was extracted with dichloromethane (DCM) three times. The combined organic layers were washed with brine and dried over Na₂SO₄. Removal of DCM and purification by silica gel column chromatography using hexane/ethyl acetate (20:1) as the eluent furnished $H_2^{\text{Me}}PDP^H$ as a yellow solid. Yield: 1.34 g, 38%. Mp: 211–213 °C. ¹H NMR (400 MHz, C_6D_6): δ 10.65 (s, 2H, NH), 7.15-7.05 (m, 3H, p-PyH and m-PyH), 6.72 (t, J = 3.2 Hz, 2H, PyH), 5.88 (m, 2H, PhH), 1.64 (s, 6H, CH₃). ¹³C NMR (101 MHz, C_6D_6): δ 151.27, 138.17, 131.50, 129.65, 114.11, 109.84, 109.21, 12.22. HRMS (ESI). Calcd for $C_{15}H_{16}N_3^+$ ([M + H]⁺): m/z238.13387. Found: *m/z* 238.13378.

2,6-Bis(1H-pyrrol-2-yl)pyridine ($H_2^H PDP^H$). The synthesis was carried out according to a modified literature procedure. 36,52 2,6-Dibromopyridine (3.6 g, 15.20 mmol, 1.00 equiv), 1-(tertbutoxycarbonyl)-2-pyrroleboronic acid (9.4 g, 44.53 mmol, 2.93 equiv), K2CO3 (18.90 g, 136.77 mmol, 9.00 equiv), and Pd(PPh3)4 (878 mg, 0.760 mmol, 0.05 equiv) were placed in a 250 mL flask under an argon atmosphere. Then, 80 mL of a deaerated toluene/ ethanol/H2O (9:3:4) solution was added via cannula transfer. The reaction mixture was heated at 90 °C under argon for 24 h. After cooling to room temperature, the solvent was removed. The residue was extracted with ethyl acetate and then passed through silica gel to remove boronic acid and palladium compounds. After removal of the solvent, the residue was treated with ethylene glycol (50 mL) and heated at 160 °C for 1 h under an argon atmosphere. After cooling to room temperature, the mixture was extracted with CHCl3. The organic layer was washed with H2O and brine and then dried over Na₂SO₄. Removal of CHCl₃ and recrystallization from CHCl₃ and hexane furnished H₂^HPDP^H as a green-yellow solid. Yield: 1.922 g, 60%; one crop. Mp: 189–191 °C. ¹H NMR (400 MHz, CDCl₃): δ 9.65 (s, 2H, NH), 7.61 (t, J = 8.0 Hz, 1H, PyH), 7.34 (d, J = 8.0 Hz, 2H, PyH), 6.90 (m, 2H, PyH), 6.74 (m, 2H, PyH), 6.31 (m, 2H,

PyH). ¹³C NMR (101 MHz, CDCl₃): δ 149.76, 137.32, 131.56, 119.71, 115.34, 110.45, 107.53. HRMS (ESI). Calcd for C₁₃H₁₂N₃⁺ ([M + H]⁺): m/z 210.10257. Found: m/z 210.10249.

2,6-Bis(3,5-dimethyl-1H-pyrrol-2-yl)pyridine $(H_2^{Me}PDP^{Me})$. The synthesis was carried out according to a modified literature procedure.⁵⁴ Bis(aminomethyl)pyridine (2.44 g, 17.79 mmol, 1.00 equiv), acetylacetone (3.65 g, 36.46 mmol, 2.05 equiv), and ptoluenesulfonic acid hydrate (2.14 g, 12.45 mmol, 0.70 equiv) were added to a 250 mL flask charged with 150 mL of xylene. The reaction flask was fitted with a Dean-Stark trap and a reflux condenser. The mixture was refluxed for 4 days. After it was cooled, the crude material was passed through a column of silica. Removal of xylene and recrystallization from ethyl acetate and hexane furnished H₂^{Me}PDP^{Me} as a yellow solid. Yield: 527 mg, 11%; one crop. Mp: 203-205 °C. ¹H NMR (400 MHz, C_6D_6): δ 10.19 (s, 2H, NH), 7.29 (dd, J = 8.8 and 7.2 Hz, 1H, p-PyH), 7.18 (d, J = 8.0 Hz, 2H, m-PyH), 5.75 (d, J = 2.8Hz, 2H, PyH), 2.34 (s, 6H, CH₃), 1.69 (s, 6H, CH₃). ¹³C NMR (101 MHz, C_6D_6): δ 151.90, 137.57, 129.44, 125.90, 120.63, 114.81, 112.35, 14.57 (d, I = 2.6 Hz), 12.24. HRMS (ESI). Calcd for $C_{17}H_{20}N_3^+$ ([M + H]⁺): m/z 266.16517. Found: m/z 266.16491.

2.6-Bis(5-methyl-3-pentafluorophenyl-1H-pyrrol-2-yl)pyridine $(H_2^{Me}PDP^{C_0F_5})$. The synthesis was carried out according to a modified literature procedure. ^{36,52} A 250 mL Schlenk flask was charged with 2,6-pyridinedicarboxaldehyde (1.000 g, 7.400 mmol, 1.00 equiv), (E)-4-pentafluorophenylbut-3-en-2-one (3.530 g, 14.95 mmol, 2.02 equiv), and 3-benzyl-5-(2-hydroxyethyl)-4-methylthiazolium chloride (1.198 g, 4.44 mmol, 0.60 equiv) under an argon atmosphere. Absolute ethanol was added followed by a solution of sodium tertbutoxide (0.427 g, 4.44 mmol, 0.60 equiv) in ethanol via a syringe. The mixture was refluxed for 24 h. Following cooling to room temperature and opening to air, ammonium acetate (3.423 g, 44.4 mmol, 6.00 equiv) was added to the mixture. The reaction mixture was again refluxed for 24 h. The resulting orange-red solution was reduced to a thick goo via rotary evaporation. This was then dissolved in ethyl acetate and washed twice with a saturated sodium bicarbonate solution, twice with H₂O, and twice with brine. Removal of ethyl acetate and purification by silica gel column chromatography using hexane/ethyl acetate (8:1) as the eluent furnished $H_2^{Me} PDP^{C_6 F_5}$ as an orange-yellow solid. Yield: 1.611 g, 76%. Mp: 184-186 °C. ¹H NMR (400 MHz, C_6D_6): δ 9.02 (s, 2H, NH), 6.88 (t, I = 7.6 Hz, 1H, PyH), 6.66 (d, J = 8.0 Hz, 2H, PyH), 5.97 (d, J = 2.4 Hz, 2H, PyH), 1.83 (s, 6H, CH₃). 13 C NMR (101 MHz, C₆D₆): δ 150.3, 144.9 (dm, J = 245 Hz), 140.4 (dm, J = 252 Hz), 138.2 (dm, J = 251 Hz), 137.6, 130.4, 128.5, 116.2, 112.7 (td, J = 18.4 and 3.8 Hz), 111.7, 107.4, 12.4. ¹⁹F NMR (376 MHz, C_6D_6): δ –140.1 (dd, J = 23.7 and 7.9 Hz), –156.7 (t, J = 21.8 Hz), -162.6 (td, J = 23.7 and 8.3 Hz). HRMS (ESI).Calcd for $C_{27}H_{14}F_{10}N_3^+$ ([M + H]⁺): m/z 570.10226. Found: m/z

 $Zr(^{Me}PDP^{C_oF_o})_2$. LiHMDS (181 mg, 1.08 mmol, 2.02 equiv) in THF was added slowly to a 20 mL vial charged with a solution of $H_2^{\ Me} PDP^{C_oF_5}$ (300 mg, 0.527 mmol, 1.00 equiv) in 3 mL of THF. The reaction was stirred for 2 h at room temperature to generate a luminescent dark-green-yellow solution of the deprotonated ligand. A suspension of ZrCl₄ (64 mg, 0.274 mmol, 0.52 equiv) in 3 mL of THF was added in small portions to the deprotonated ligand over 20 min. The reaction mixture was allowed to stir at room temperature, and the color of the solution slowly changed to emissive red. After 2 days, THF was removed in vacuo and the residue triturated with diethyl ether (Et₂O) three times. The solid residue was then dissolved in a minimum amount of ether and filtered through Celite. The crude product was purified by recrystallization [pentane/ether (2:1)] at -35⁶C. Yield: 207 mg, 63%. ¹H NMR (400 MHz, C_6D_6): δ 6.73 (t, J = 8.0 Hz, 2H, PyH), 6.41 (d, I = 7.6 Hz, 4H, PyH), 5.70 (s, 4H, PyH), 2.08 (s, 12H, CH₃). ¹³C NMR (100 MHz, C₆D₆): δ 154.2, 144.6 (dm, J = 246 Hz), 143.4, 141.6, 140.7 (dm, J = 252 Hz), 138.2 (dm, J = 247 Hz), 137.2, 114.5, 112.5, 111.5, 111.3 (td, I = 18.7 and 3.5 Hz), 14.3. ¹⁹F NMR (376 MHz, C_6D_6): δ –139.6 (dd, J = 24.1 and 7.9 Hz), -155.2 (t, J = 21.4 Hz), -162.0 (td, J = 23.7 and 7.9 Hz). Anal. Calcd for $C_{54}H_{22}F_{20}N_6Zr$: C, 52.90; H, 1.81; N, 6.85. Found: C, 52.79; H, 1.71; N, 6.62. Single crystals suitable for X-ray crystallographic

analysis were grown from a pentane/Et₂O (2:1) solution of $Zr(^{Me}PDP^{C_6F_5})_2$ at -35 °C.

 $Zr(^HPDP^H)_2$. A solution of tetrabenzylzirconium (109 mg, 0.239 mmol, 1.00 equiv) in 1 mL of toluene was added slowly to a 20 mL vial charged with a solution of H_2^{HPDPH} (100 mg, 0.478 mmol, 2.00 equiv) in 2 mL of benzene. The reaction was stirred for 10 min at room temperature, and the desired product crystallized out with stirring. The reaction was then filtered, and the solid was washed three times with benzene. The product was collected as a dark-orange microcrystalline solid. Yield: 110 mg, 91%. 1H NMR (400 MHz, C_6D_6): δ 6.83 (t, J = 8.0 Hz, 2H, p-PyH), 6.80 (d, J = 1.6 Hz, 4H, PyH), 6.54 (dd, J = 3.2 and 0.8 Hz, 4H, PyH), 6.44 (d, J = 8.0 Hz, 2H, m-PyH), 6.06 (t, J = 2.8 Hz, 4H, PyH). 13 C NMR (101 MHz, C_6D_6): δ 154.63, 142.64, 140.56, 131.44, 112.00, 111.55, 111.23. Anal. Calcd for $C_2GH_{18}N_6Zr$: C, 61.75; H, 3.59; N, 16.62. Found: C, 61.59; H, 3.98; N, 16.33. Single crystals suitable for X-ray crystallographic analysis were grown from a saturated solution of $Zr(^HPDP^H)_2$ in C_6D_6 at room temperature.

 $Zr(^{H}PDP^{H})_{2}$ in $C_{6}D_{6}$ at room temperature. $Zr(^{\rho h}PDP^{\rho h})_{2}$. n-BuLi [0.499 mL (1.6 M solution in hexanes), 0.798 mmol, 2.05 equiv] was added slowly to a 20 mL vial charged with a solution of H₂^{Me}PDP^H (200 mg, 0.389 mmol, 1.00 equiv) in 5 mL of THF. The reaction was stirred for 2 h at room temperature to generate a luminescent dark-red-orange solution of the deprotonated ligand. A solution of ZrCl₄ (47 mg, 0.202 mmol, 0.52 equiv) in 3 mL of THF was added in small portions to the deprotonated ligand over 20 min. The reaction mixture was allowed to stir at room temperature, and the color of the solution slowly changed to emissive red. After 2 days, THF was removed in vacuo and triturated with Et₂O three times. The solid residue was washed three times with benzene to remove any unreacted $\text{Li}_2^{\ Ph} PDP^{Ph}$ and potential monoligated zirconium species. The crude product was dried in vacuo, redissolved in DCM, and filtered to remove LiCl and potentially unreacted ZrCl4. Removal of the solvent in vacuo followed by recrystallization from Et₂O at -35 °C provided a red microcrystalline solid. Yield: 176 mg, 81%. ¹H NMR (600 MHz, CDCl₃): δ 7.44–7.37 (m, 16H, PhH), 7.35-7.28 (m, 12H, PhH), 6.97-6.89 (m, 12H, PhH), 6.81 (t, J = 7.8Hz, 2H, p-PyH), 6.35 (d, J = 7.8 Hz, 4H, PyH), 6.09 (s, 4H, PyH). ¹³C NMR (151 MHz, CDCl₃): δ 153.56, 145.66, 140.13, 136.82, 135.78, 135.49, 129.27, 129.26, 128.42, 128.24, 126.97, 126.85, 126.77, 113.73, 113.00. Anal. Calcd for C₇₄H₅₀N₆Zr·Et₂O: C, 78.82; H, 5.09; N, 7.07. Found: C, 79.10; H, 5.16; N, 7.22. Single crystals suitable for X-ray crystallographic analysis were grown from a saturated Et₂O solution of Zr(PhPDPPh)₂ at -35 °C.

 $Zr(^{Me}PDP^{\tilde{H}})_2$. n-BuLi [2.23 mL (1.6 M solution in hexanes), 3.58 mmol, 2.02 equiv] was added slowly to a 20 mL vial charged with a solution of H₂^{Me}PDP^H (420 mg, 1.77 mmol, 1.00 equiv) in 5 mL of THF. The reaction was stirred for 2 h at room temperature to generate a luminescent dark-green-orange solution of the deprotonated ligand. A solution of ZrCl₄ (227 mg, 0.973 mmol, 0.55 equiv) in 3 mL of THF was added in small portions to the deprotonated ligand over 20 min. The reaction mixture was allowed to stir at room temperature, and the color of the solution slowly changed to emissive red. After 2 days, THF was removed in vacuo and triturated with Et₂O three times. The solid residue was washed three times with Et₂O to remove any unreacted Li2 MePDPH and potential monoligated zirconium species. The crude product was dried in vacuo, redissolved in DCM, and filtered to remove LiCl and potentially unreacted ZrCl4. Removal of the solvent in vacuo provided a red microcrystalline solid. Yield: 283 mg, 57%. ¹H NMR (400 MHz, C_6D_6): δ 6.83 (t, J = 8.0Hz, 2H, p-PyH), 6.53 (d, J = 3.2 Hz, 4H, PyH), 6.45 (d, J = 8.0 Hz, 4H, m-PyH), 5.76 (dd, J = 3.2 and 0.8 Hz, 4H, PyH), 2.01 (s, 12H, CH_3). ¹³C NMR (101 MHz, C_6D_6): δ 154.72, 142.39, 141.93, 140.25, 111.83, 111.01, 110.36, 14.70. Anal. Calcd for $C_{30}H_{26}N_6Zr^{-1}/_6DCM$: C, 62.91; H, 4.61; N, 14.59. Found: C, 63.17; H, 4.59; N, 14.36. Single crystals suitable for X-ray crystallographic analysis were grown from a pentane/THF (1:1) solution of Zr(MePDPH)₂ at -35 °C.

 $Zr(^{Me}PDP^{Me})_2$. n-BuLi [2.54 mL (1.6 M solution in hexanes), 4.07 mmol, 2.05 equiv] was added slowly to a 20 mL vial charged with a solution of $H_2^{Me}PDP^{Me}$ (527 mg, 1.99 mmol, 1.00 equiv) in 5 mL of THF. The reaction was stirred for 2 h at room temperature to

generate a luminescent dark-green-orange solution of the deprotonated ligand. A solution of ZrCl₄ (241 mg, 1.03 mmol, 0.52 equiv) in 3 mL of THF was added in small portions to the deprotonated ligand over 20 min. The reaction mixture was allowed to stir at room temperature, and the color of the solution slowly changed to emissive red. After 2 days, THF was removed in vacuo and triturated with Et₂O three times. The solid residue was washed three times with Et₂O to remove any unreacted Li2 MePDPMe and potential monoligated zirconium species. The crude product was dried in vacuo, redissolved in DCM, and filtered to remove LiCl and potentially unreacted ZrCl₄. Removal of the solvent in vacuo provided a red microcrystalline solid. Yield: 494 mg, 81%. ¹H NMR ($\hat{4}00$ MHz, CDCl₃): δ 7.54 (t, J = 8.0Hz, 2H, p-PyH), 6.87 (d, J = 8.0 Hz, 4H, m-PyH), 5.52 (s, 4H, PyH), 2.27 (s, 12H, CH₃), 1.86 (s, 12H, CH₃). ¹³C NMR (101 MHz, CDCl₂): δ 154.87, 141.77, 140.71, 135.86, 124.29, 113.22, 110.43, 14.49, 13.35. Anal. Calcd for C₃₄H₃₄N₆Zr: C, 66.09; H, 5.55; N, 13.60. Found: C, 65.83; H, 5.47; N, 13.38. Single crystals suitable for X-ray crystallographic analysis were grown from a dilute THF solution of $Zr(^{Me}PDP^{Me})_2$ at -35 °C.

ASSOCIATED CONTENT

Supporting Information

The Supporting Information is available free of charge at https://pubs.acs.org/doi/10.1021/acs.inorgchem.0c02343.

Additional experimental procedures, spectroscopic and crystallographic data, and computational details (PDF)

Accession Codes

CCDC 2021670–2021675 contain the supplementary crystallographic data for this paper. These data can be obtained free of charge via www.ccdc.cam.ac.uk/data_request/cif, or by emailing data_request@ccdc.cam.ac.uk, or by contacting The Cambridge Crystallographic Data Centre, 12 Union Road, Cambridge CB2 1EZ, UK; fax: +44 1223 336033.

AUTHOR INFORMATION

Corresponding Author

Carsten Milsmann — C. Eugene Bennett Department of Chemistry, West Virginia University (WVU), Morgantown, West Virginia 26506, United States; ⊚ orcid.org/0000-0002-9249-5199; Email: camilsmann@mail.wvu.edu

Authors

Yu Zhang — C. Eugene Bennett Department of Chemistry, West Virginia University (WVU), Morgantown, West Virginia 26506, United States; Orcid.org/0000-0001-8948-1434

Dylan C. Leary — C. Eugene Bennett Department of Chemistry, West Virginia University (WVU), Morgantown, West Virginia 26506, United States; Occid.org/0000-0003-0588-8267

Anne M. Belldina — C. Eugene Bennett Department of Chemistry, West Virginia University (WVU), Morgantown, West Virginia 26506, United States

Jeffrey L. Petersen – C. Eugene Bennett Department of Chemistry, West Virginia University (WVU), Morgantown, West Virginia 26506, United States

Complete contact information is available at: https://pubs.acs.org/10.1021/acs.inorgchem.0c02343

Notes

The authors declare no competing financial interest.

ACKNOWLEDGMENTS

We thank WVU and the National Science Foundation (Grant CHE-1752738) for financial support. This work used X-ray crystallography (Grant CHE-1336071) and NMR (Grant

CHE-1228336) equipment funded by the National Science Foundation. The WVU High Performance Computing facilities are funded by the National Science Foundation EPSCoR Research Infrastructure Improvement Cooperative Agreement 1003907, the State of West Virginia (WVEPSCoR via the Higher Education Policy Commission), the WVU Research Corporation, and faculty investments.

REFERENCES

- (1) Zhang, S.; Yang, X.; Numata, Y.; Han, L. Highly Efficient Dye-Sensitized Solar Cells: Progress and Future Challenges. *Energy Environ. Sci.* **2013**, *6*, 1443–1464.
- (2) Grätzel, M. Dye-Sensitized Solar Cells. J. Photochem. Photobiol., C 2003, 4, 145–153.
- (3) Hagfeldt, A.; Boschloo, G.; Sun, L.; Kloo, L.; Pettersson, H. Dye-Sensitized Solar Cells. *Chem. Rev.* **2010**, *110*, 6595–6663.
- (4) Nazeeruddin, M. K.; Baranoff, E.; Grätzel, M. Dye-Sensitized Solar Cells: A Brief Overview. *Sol. Energy* **2011**, *85*, 1172–1178.
- (5) Yersin, H.; Rausch, A. F.; Czerwieniec, R.; Hofbeck, T.; Fischer, T. The Triplet State of Organo-Transition Metal Compounds. Triplet Harvesting and Singlet Harvesting for Efficient OLEDs. *Coord. Chem. Rev.* 2011, 255, 2622–2652.
- (6) Xu, H.; Chen, R.; Sun, Q.; Lai, W.; Su, Q.; Huang, W.; Liu, X. Recent Progress in Metal-Organic Complexes for Optoelectronic Applications. *Chem. Soc. Rev.* **2014**, *43*, 3259–3302.
- (7) Prier, C. K.; Rankic, D. A.; MacMillan, D. W. C. Visible Light Photoredox Catalysis with Transition Metal Complexes: Applications in Organic Synthesis. *Chem. Rev.* **2013**, *113*, 5322–5363.
- (8) Arias-Rotondo, D. M.; McCusker, J. K. The Photophysics of Photoredox Catalysis: A Roadmap for Catalyst Design. *Chem. Soc. Rev.* **2016**, *45*, 5803–5820.
- (9) Glaser, F.; Wenger, O. S. Recent Progress in the Development of Transition-Metal Based Photoredox Catalysts. *Coord. Chem. Rev.* **2020**, 405, 213129.
- (10) Romero, N. A.; Nicewicz, D. A. Organic Photoredox Catalysis. *Chem. Rev.* **2016**, *116*, 10075–10166.
- (11) Xuan, J.; Xiao, W.-J. Visible-Light Photoredox Catalysis. Angew. Chem., Int. Ed. 2012, 51, 6828–6838.
- (12) Angnes, R. A.; Li, Z.; Correia, C. R. D.; Hammond, G. B. Recent Synthetic Additions to the Visible Light Photoredox Catalysis Toolbox. *Org. Biomol. Chem.* **2015**, *13*, 9152–9167.
- (13) Zeitler, K. Photoredox Catalysis with Visible Light. Angew. Chem., Int. Ed. 2009, 48, 9785–9789.
- (14) Tucker, J. W.; Stephenson, C. R. J. Shining Light on Photoredox Catalysis: Theory and Synthetic Applications. *J. Org. Chem.* **2012**, *77*, 1617–1622.
- (15) Larsen, C. B.; Wenger, O. S. Photoredox Catalysis with Metal Complexes Made from Earth-Abundant Elements. *Chem. Eur. J.* **2018**, 24, 2039–2058.
- (16) Nocera, D. G. Solar Fuels and Solar Chemicals Industry. Acc. Chem. Res. 2017, 50, 616-619.
- (17) For recent reviews, see the special issue on Solar Fuels: *Chem. Soc. Rev.* **2013**, 2205–2472.
- (18) Monro, S.; Colón, K. L.; Yin, H.; Roque, J.; Konda, P.; Gujar, S.; Thummel, R. P.; Lilge, L.; Cameron, C. G.; McFarland, S. A. Transition Metal Complexes and Photodynamic Therapy from a Tumor-Centered Approach: Challenges, Opportunities, and Highlights from the Development of TLD1433. *Chem. Rev.* **2019**, *119*, 797–828.
- (19) Förster, C.; Heinze, K. Photophysics and Photochemistry with Earth-Abundant Metals-Fundamentals and Concepts. *Chem. Soc. Rev.* **2020**, *49*, 1057–1070.
- (20) Mara, M. W.; Fransted, K. A.; Chen, L. X. Interplays of Excited State Structures and Dynamics in Copper(I) Diimine Complexes: Implications and Perspectives. *Coord. Chem. Rev.* **2015**, 282–283, 2–18.

- (21) Iwamura, M.; Takeuchi, S.; Tahara, T. Ultrafast Excited-State Dynamics of Copper(I) Complexes. *Acc. Chem. Res.* **2015**, *48*, 782–791.
- (22) Lazorski, M. S.; Castellano, F. N. Advances in the Light Conversion Properties of Cu(I)-Based Photosensitizers. *Polyhedron* **2014**, *82*, 57–70.
- (23) Cunningham, C. T.; Cunningham, K. L. H.; Michalec, J. F.; Mcmillin, D. R. Cooperative Substituent Effects on the Excited States of Copper Phenanthrolines. *Inorg. Chem.* **1999**, *38*, 4388–4392.
- (24) Büldt, L. A.; Guo, X.; Vogel, R.; Prescimone, A.; Wenger, O. S. A Tris(Diisocyanide)Chromium(0) Complex Is a Luminescent Analog of Fe(2,2'-Bipyridine)₃²⁺. *J. Am. Chem. Soc.* **2017**, 139, 985–992.
- (25) Büldt, L. A.; Wenger, O. S. Chromium(0), Molybdenum(0), and Tungsten(0) Isocyanide Complexes as Luminophores and Photosensitizers with Long-Lived Excited States. *Angew. Chem., Int. Ed.* **2017**, *56*, 5676–5682.
- (26) Otto, S.; Grabolle, M.; Förster, C.; Kreitner, C.; Resch-Genger, U.; Heinze, K. [Cr(Ddpd)₂]³⁺: A Molecular, Water-Soluble, Highly NIR-Emissive Ruby Analogue. *Angew. Chem., Int. Ed.* **2015**, *54*, 11572–11576.
- (27) Wang, C.; Otto, S.; Dorn, M.; Kreidt, E.; Lebon, J.; Sršan, L.; Di Martino-Fumo, P.; Gerhards, M.; Resch-Genger, U.; Seitz, M.; Heinze, K. Deuterated Molecular Ruby with Record Luminescence Quantum Yield. *Angew. Chem., Int. Ed.* **2018**, *57*, 1112–1116.
- (28) Treiling, S.; Wang, C.; Förster, C.; Reichenauer, F.; Kalmbach, J.; Boden, P.; Harris, J. P.; Carrella, L. M.; Rentschler, E.; Resch-Genger, U.; Reber, C.; Seitz, M.; Gerhards, M.; Heinze, K. Luminescence and Light-Driven Energy and Electron Transfer from an Exceptionally Long-Lived Excited State of a Non-Innocent Chromium(III) Complex. *Angew. Chem., Int. Ed.* **2019**, *58*, 18075—18085.
- (29) Fredin, L. A.; Pápai, M.; Rozsályi, E.; Vankó, G.; Wärnmark, K.; Sundström, V.; Persson, P. Exceptional Excited-State Lifetime of an Iron(II)- N -Heterocyclic Carbene Complex Explained. *J. Phys. Chem. Lett.* **2014**, *5*, 2066–2071.
- (30) Chábera, P.; Kjaer, K. S.; Prakash, O.; Honarfar, A.; Liu, Y.; Fredin, L. A.; Harlang, T. C. B.; Lidin, S.; Uhlig, J.; Sundström, V.; Lomoth, R.; Persson, P.; Wärnmark, K. FeII Hexa N-Heterocyclic Carbene Complex with a 528 Ps Metal-To-Ligand Charge-Transfer Excited-State Lifetime. *J. Phys. Chem. Lett.* 2018, 9, 459–463.
- (31) Kjær, K. S.; Styring, S.; Persson, P.; Honarfar, A.; Uhlig, J.; Ericsson, T.; Bendix, J.; Bergquist, K.-E.; Wärnmark, K.; Prakash, O.; Yartsev, A.; Rosemann, N. W.; Gordivska, O.; Chábera, P.; Strand, D.; Lindh, L.; Kaul, N.; Lomoth, R.; Fredin, L. A.; Häggström, L.; Huang, P.; Sundström, V. Luminescence and Reactivity of a Charge-Transfer Excited Iron Complex with Nanosecond Lifetime. *Science* **2019**, *363*, 249–253.
- (32) Chábera, P.; Liu, Y.; Prakash, O.; Thyrhaug, E.; Nahhas, A. El; Honarfar, A.; Essén, S.; Fredin, L. A.; Harlang, T. C. B.; Kjær, K. S.; Handrup, K.; Ericson, F.; Tatsuno, H.; Morgan, K.; Schnadt, J.; Häggström, L.; Ericsson, T.; Sobkowiak, A.; Lidin, S.; Huang, P.; Styring, S.; Uhlig, J.; Bendix, J.; Lomoth, R.; Sundström, V.; Persson, P.; Wärnmark, K. A Low-Spin Fe(III) Complex with 100-Ps Ligand-to-Metal Charge Transfer Photoluminescence. *Nature* **2017**, *543*, 695–699.
- (33) Ashford, D. L.; Glasson, C. R. K.; Norris, M. R.; Concepcion, J. J.; Keinan, S.; Brennaman, M. K.; Templeton, J. L.; Meyer, T. J. Controlling Ground and Excited State Properties through Ligand Changes in Ruthenium Polypyridyl Complexes. *Inorg. Chem.* **2014**, 53, 5637–5646.
- (34) Motley, T. C.; Troian-Gautier, L.; Brennaman, M. K.; Meyer, G. J. Excited-State Decay Pathways of Tris(Bidentate) Cyclometalated Ruthenium(II) Compounds. *Inorg. Chem.* **2017**, *56*, 13579–13592.
- (35) Zhang, X. Z.; Cheng, C. C.; Chih, Y. R.; Lin, Y. T.; Chen, H. Y.; Chen, Y. J.; Endicott, J. F. Low-Temperature Spectra and Density Functional Theory Modeling of Ru(II)-Bipyridine Complexes with Cyclometalated Ancillary Ligands: The Excited State Spin-Orbit

- Coupling Origin of Variations in Emission Efficiencies. *J. Phys. Chem.* A **2019**, *123*, 9431–9449.
- (36) Zhang, Y.; Petersen, J. L.; Milsmann, C. A Luminescent Zirconium(IV) Complex as a Molecular Photosensitizer for Visible Light Photoredox Catalysis. *J. Am. Chem. Soc.* **2016**, *138*, 13115—13118
- (37) Zhang, Y.; Lee, T. S.; Petersen, J. L.; Milsmann, C. A Zirconium Photosensitizer with a Long-Lived Excited State: Mechanistic Insight into Photo-Induced Single Electron Transfer. *J. Am. Chem. Soc.* **2018**, 140, 5934–5947.
- (38) Zhang, Y.; Lee, T. S.; Favale, J. M.; Leary, D. C.; Petersen, J. L.; Scholes, G. D.; Castellano, F. N.; Milsmann, C. Delayed Fluorescence from a Zirconium(IV) Photosensitizer with Ligand-to-Metal Charge-Transfer Excited States. *Nat. Chem.* **2020**, *12*, 345.
- (39) Pfennig, B. W.; Thompson, M. E.; Bocarsly, A. B. A New Class of Room Temperature Luminescent Organometallic Complexes: Luminescence and Photophysical Properties of Permethylscandocene Chloride in Fluid Solution. *J. Am. Chem. Soc.* **1989**, *111*, 8947–8948.
- (40) Paulson, S.; Sullivan, B. P.; Caspar, J. V. Luminescent Ligand-to-Metal Charge-Transfer Excited States Based on Pentamethylcyclopentadienyl Complexes of Tantalum. *J. Am. Chem. Soc.* **1992**, *114*, 6905–6906.
- (41) Heinselman, K. S.; Hopkins, M. D. Luminescence Properties of d⁰ Metal-Imido Compounds. *J. Am. Chem. Soc.* **1995**, *117*, 12340–12341.
- (42) Loukova, G. V.; Smirnov, V. A. Phosphorescent Ligand-to-Metal Charge-Transfer Excited States in the Group IVB Metallocene Triad. *Chem. Phys. Lett.* **2000**, 329, 437–442.
- (43) Loukova, G. V.; Smirnov, V. A. Phosphorescence of Group IVB Metal Complexes. *Russ. Chem. Bull.* **2001**, *50*, 329–330.
- (44) Loukova, G. V.; Vasiliev, V. P.; Smirnov, V. A. Intense Luminescence of the Group IVB Metal π -Complex in Solutions at Room Temperature. *Russ. Chem. Bull.* **2007**, *56*, 181–182.
- (45) Loukova, G. V.; Huhn, W.; Vasiliev, V. P.; Smirnov, V. A. Ligand-to-Metal Charge Transfer Excited States with Unprecedented Luminescence Yield in Fluid Solution. *J. Phys. Chem. A* **2007**, *111*, 4117–4121.
- (46) Loukova, G. V.; Milov, A. A.; Vasiliev, V. P.; Minkin, V. I. Nature of Ligand to Metal Charge Transfer States in the Metallocene Series $M(\eta^5:\eta^1-CpCMe_2CB_{10}H_{10}C)_2$ (M = Ti, Zr, Hf). Russ. Chem. Bull. 2017, 66, 1325–1327.
- (47) Loukova, G. V.; Milov, A. A.; Vasiliev, V. P.; Minkin, V. I. Frontier Orbitals and Ligand-to-Metal Charge Transfer Electronic Transitions in d⁰-Metal Complexes. *High Energy Chem.* **2017**, *51*, 333–337.
- (48) Romain, C.; Choua, S.; Collin, J. P.; Heinrich, M.; Bailly, C.; Karmazin-Brelot, L.; Bellemin-Laponnaz, S.; Dagorne, S. Redox and Luminescent Properties of Robust and Air-Stable N-Heterocyclic Carbene Group 4 Metal Complexes. *Inorg. Chem.* **2014**, *53*, 7371–7376.
- (49) Gazi, S.; Hung Ng, W. K.; Ganguly, R.; Putra Moeljadi, A. M.; Hirao, H.; Soo, H. S. Selective Photocatalytic C-C Bond Cleavage under Ambient Conditions with Earth Abundant Vanadium Complexes. *Chem. Sci.* **2015**, *6*, 7130–7142.
- (50) Wenger, O. S. Photoactive Complexes with Earth-Abundant Metals. J. Am. Chem. Soc. 2018, 140, 13522–13533.
- (51) Hockin, B. M.; Li, C.; Robertson, N.; Zysman-Colman, E. Photoredox Catalysts Based on Earth-Abundant Metal Complexes. *Catal. Sci. Technol.* **2019**, *9*, 889–915.
- (52) Hakey, B. M.; Darmon, J. M.; Zhang, Y.; Petersen, J. L.; Milsmann, C. Synthesis and Electronic Structure of Neutral Square-Planar High- Spin Iron(II) Complexes Supported by a Dianionic Pincer Ligand. *Inorg. Chem.* **2019**, *58*, 1252–1266.
- (53) Jones, R. A.; Karatza, M.; Voro, T. N.; Civeir, P. U.; Franck, A.; Ozturk, O.; Seaman, J. P.; Whitmore, A. P.; Williamson, D. J. Extended Heterocyclic Systems 1. The Synthesis and Characterisation of Pyrrolylpyridines, Alternating Pyrrole: Pyridine Oligomers and Polymers, and Related Systems. *Tetrahedron* **1996**, *52*, 8707–8724.

- (54) Komine, N.; Buell, R. W.; Chen, C.-H.; Hui, A. K.; Pink, M.; Caulton, K. G. Probing the Steric and Electronic Characteristics of a New Bis-Pyrrolide Pincer Ligand. *Inorg. Chem.* **2014**, *53*, 1361–1369.
- (55) Würth, C.; Grabolle, M.; Pauli, J.; Spieles, M.; Resch-Genger, U. Relative and Absolute Determination of Fluorescence Quantum Yields of Transparent Samples. *Nat. Protoc.* **2013**, *8*, 1535–1550.
- (56) Brouwer, A. M. Standards for Photoluminescence Quantum Yield Measurements in Solution (IUPAC Technical Report). *Pure Appl. Chem.* **2011**, *83*, 2213–2228.
- (\$7) Gowda, A. S.; Petersen, J. L.; Milsmann, C. Redox Chemistry of Bis(Pyrrolyl)Pyridine Chromium and Molybdenum Complexes: An Experimental and Density Functional Theoretical Study. *Inorg. Chem.* **2018**, *57*, 1919–1934.
- (58) Zhu, X.-Q.; Zhang, M.-T.; Yu, A.; Wang, C.-H.; Cheng, J.-P. Hydride, Hydrogen Atom, Proton, and Electron Transfer Driving Forces of Various Five-Membered Heterocyclic Organic Hydrides and Their Reaction Intermediates in Acetonitrile. *J. Am. Chem. Soc.* **2008**, 130, 2501–2516.
- (59) Nguyen, J. D.; D'Amato, E. M.; Narayanam, J. M. R.; Stephenson, C. R. J. Engaging Unactivated Alkyl, Alkenyl and Aryl Iodides in Visible-Light-Mediated Free Radical Reactions. *Nat. Chem.* **2012**, *4*, 854.
- (60) Cowper, N. G. W.; Chernowsky, C. P.; Williams, O. P.; Wickens, Z. K. Potent Reductants via Electron-Primed Photoredox Catalysis: Unlocking Aryl Chlorides for Radical Coupling. *J. Am. Chem. Soc.* **2020**, *142*, 2093–2099.
- (61) Radlauer, M. R.; Agapie, T. Bimetallic Zirconium Amine Bis(Phenolate) Polymerization Catalysts: Enhanced Activity and Tacticity Control for Polyolefin Synthesis. *Organometallics* **2014**, 33, 3247–3250.
- (62) Rong, Y.; Al-Harbi, A.; Parkin, G. Highly Variable Zr-CH₂-Ph Bond Angles in Tetrabenzylzirconium: Analysis of Benzyl Ligand Coordination Modes. *Organometallics* **2012**, *31*, 8208–8217.